International Journal of Bifurcation and Chaos

The structure of invariant tori in a 3D galactic potential

M. KATSANIKAS
Research Center for Astronomy, Academy of Athens
Soranou Efessiou 4, GR-11527 Athens, Greece

Section of Astrophysics, Astronomy and Mechanics,
Department of Physics, University of Athens, Greece
mkatsan@academyofathens.gr

P.A. PATSIS
Research Center for Astronomy, Academy of Athens
Soranou Efessiou 4, GR-11527 Athens, Greece
patsis@academyofathens.gr

Received (to be inserted by publisher)

We study in detail the structure of phase space in the neighborhood of stable periodic orbits in a rotating 3D potential of galactic type. We have used the color and rotation method to investigate the properties of the invariant tori in the 4D spaces of section. We compare our results with those of previous works and we describe the morphology of the rotational, as well as of the tube tori in the 4D space. We find sticky chaotic orbits in the immediate neighborhood of sets of invariant tori surrounding 3D stable periodic orbits. Particularly useful for galactic dynamics is the behavior of chaotic orbits trapped for long time between 4D invariant tori. We find that they support during this time the same structure as the quasi-periodic orbits around the stable periodic orbits, contributing however to a local increase of the dispersion of velocities. Finally we find that the tube tori do not appear in the 3D projections of the spaces of section in the axisymmetric Hamiltonian we examined.

Keywords: Chaos and Dynamical Systems, Galactic Dynamics, 4D surfaces of section, Invariant tori

1. Introduction

The method of surfaces of section for the study of dynamical systems dates back to Poincaré (1892) and has many applications to Dynamical Astronomy (for a review see e.g. Contopoulos 2002). A basic problem in Hamiltonian Systems of three degrees of freedom is the visualization of the 4D[1] surfaces of section. Let us assume the phase space of an autonomous Hamiltonian system, that has 6 dimensions, e.g. in Cartesian coordinates, $(x, y, z, \dot{x}, \dot{y}, \dot{z})$. For a given value of the Hamiltonian a trajectory lies on a 5D manifold. In this manifold a surface of section is 4D. This does not allow us to visualize it directly. Several methods have been applied to overcome this problem in the past and we summarize them below.

The structure of the 4D space phase space was examined for the first time in the pioneer work of Froeschlé (1970, 1972). In that work he used stereoscopic views and the method of slices in order to understand the structure of tori, that appeared at the neighborhood of stable periodic orbits. Similar methods have been applied by Martinet and Magnenat (1981), Contopoulos et al. (1982), and Magnenat (1982) for studying the 3D projections of invariant tori in the 4D surface of section or in the phase space of a 4D symplectic map. The 2D projections of such invariant tori have been examined on various 2D planes in detail (e.g. Skokos, Contopoulos and Polymilis 1997, 1999).

In the present paper we use the method of color and rotation proposed by Patsis and Zachilas (1994). In this method we first consider 3D projections and rotate the 3D figures on a computer screen to observe the figure from all its sides. Then we use colors to indicate the 4th dimension. For this purpose we make use of the "Mathematica" package (Wolfram 1999) and of its subroutines. Each point is colored according to the value of its 4th coordinate in the following way: Firstly we define the surface of section that we will use, e.g. $y = 0$ with $\dot{y} > 0$. Secondly we select a 3D subspace of the surface of section, e.g. $(x, \dot{x}, \dot{z})$ and we determine the minimum and maximum values of the 4th coordinate z. Finally we normalize the resulting interval [min(z), max(z)] into [0,1] from which interval the color functions of "Mathematica" take values. In our figures we give always the color function of "Mathematica" that we used in a color-coded bar. The point of view of the observer of the figures is given in spherical coordinates. This specifies the direction along which the figure is projected. The unit for distance d of the consequents of the surface of section from the observer is given by "Mathematica" in a special scaled coordinate system in which the longest side of the bounding box, which surrounds the figure, has length 1. For all figures we use $d = 1$. The method associates the smooth distribution or the mixing of colors, with specific types of dynamical behavior in the 4th dimension (Patsis and Zachilas 1994).

In order to study the structure of phase space at the neighborhood of a periodic orbit (p.o.), we first locate it by means of an iterative method and calculate its stability. The calculation of the linear stability of a periodic orbit is based on the method of Broucke (1969) and Hadjidemetriou (1975). We first consider small deviations from its initial conditions and then integrate the orbit again to the next upward intersection. In this way a 4D map (Poincaré map) is established, which is unique (Abraham and Marsden 1978 p. 521) and relates the initial with the final point. The relation of the final deviations of this neighboring orbit from the periodic one, with the initially introduced deviations can be written in vector form as $\xi = \mathrm{M}\ \xi_0$. Here ξ is the final deviation, ξ_0 is the initial deviation M is a 4×4 matrix, called the monodromy matrix. This matrix satisfies the symplectic identity and the map is called symplectic (Arnold and Givental 2000). It can be shown that the characteristic equation can be written in the form $\lambda^4 + a\lambda^3 + \beta\lambda^2 + a\lambda + 1 = 0$. Its solutions $\lambda_i,\ i = 1, 2, 3, 4$, due to the symplectic identity of the monodromy matrix, that obey the relations $\lambda_1\lambda_2 = 1$ and $\lambda_3\lambda_4 = 1$ can be written as

$$\begin{aligned} \lambda_1, \frac{1}{\lambda_1} &= \frac{-b_1 \pm \sqrt{b_1^2 - 4}}{2} \\ \lambda_3, \frac{1}{\lambda_3} &= \frac{-b_2 \pm \sqrt{b_2^2 - 4}}{2} \end{aligned} \tag{1}$$

where

$$b_{1,2} = \frac{a \pm \sqrt{\Delta}}{2} \tag{2}$$

and

$$\Delta = a^2 - 4(\beta - 2) \tag{3}$$

[1] throughout the paper we will refer to "n-dimensional" as "nD"; i.e. 3D, 4D etc.

The quantities b_1 and b_2 are called the stability indices. Following the notation of Contopoulos and Magnenat (1985) if $\Delta > 0$, $|b_1| < 2$ and $|b_2| < 2$, all four eigenvalues are complex on the unit circle and the periodic orbit is called "stable" (S). If $\Delta > 0$ and $|b_1| > 2$, $|b_2| < 2$ or $|b_1| < 2$, $|b_2| > 2$, the periodic orbit is called "simple unstable" (U). In this case two eigenvalues are on the real axis and two are complex on the unit circle. If $\Delta > 0$ and $|b_1| > 2$ and $|b_2| > 2$, the periodic orbit is called "double unstable" (DU) and the four eigenvalues are on the real axis. Finally if $\Delta < 0$ the periodic orbit is called "complex unstable" (Δ). In this case the four eigenvalues are complex numbers and they are off the unit circle. For the generalization of this kind of instability in Hamiltonian systems of N degrees of freedom the reader may refer to Skokos (2001). When two eigenvalues collide at $(1, 0)$ of the unit circle the parent family becomes simple unstable (U) and a new family of p.o. is born. In this paper we examine the evolution of the phase space at the transition from stability to simple instability ($S \to U$). The parent family in our example has an orbital plane, i.e. it is 2D, and by becoming simple unstable as the energy increases, it generates by bifurcation a stable 3D family of p.o..

According to the KAM theorem (Kolmogorov 1954, Moser 1962, Arnold 1963) in an almost Integrable Hamiltonian system of N degrees of freedom there are orbits that lie on N-dimensional tori. The KAM theorem has been extended to 2n-dimensional almost integrable symplectic maps by Wiggins (2003, p.225) and by Kuksin and Pöschel (1994). This means that in a 2n-dimensional almost integrable symplectic map there are orbits that lie on n-dimensional tori. In our 3D Hamiltonian system a 4D Poincaré map is defined on the surface of section. In specific cases this 4D Poincaré map is almost integrable. Then, according to Wiggins (2003, p.225), we have orbits that lie on 2D invariant tori in the 4D space of section. The structure of these tori, is the subject of our present, rather descriptive, paper.

In order to facilitate the discussion of the figures in the paper, we give some useful definitions related to a torus. In the 3D space, a torus is a surface that is generated when we rotate a circle on the x-z (or y-z) plane around the axis z (Fig. 1). The definition of the angles u and v are also noted in Fig. 1. The internal surface of the torus is defined as the set of points of the torus, where we have $90^o \leq u \leq 270^o$. The external surface of torus is defined as the set of points of the torus, where we have $0^o \leq u \leq 90^o$ and $270^o \leq u \leq 360^o$. We will call "tori" the objects we study in this paper, despite the fact that they seem to be generated by an ellipse instead of a circle i.e. they are elliptic tori.

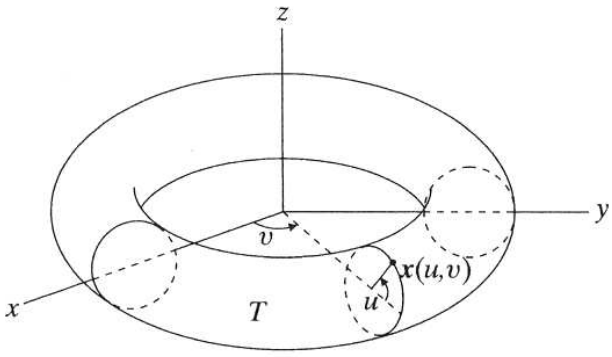

Fig. 1. The definition of the v and u angles on a torus. Arrows indicate the direction along which the angles u,v increase from zero towards larger values.

The purpose of this paper is to study the structure of the phase space in the neighborhood of stable periodic orbits in 3D galactic potentials. We want to understand how the phase space is structured and how it evolves as the stability of the x1, 2D central family of our system on the equatorial plane, changes from stable to simple unstable. We want also to understand how the phase space structure evolves as the main parameters of our system vary. In section 2 we describe our Hamiltonian system, while in section 3 we present the morphological evolution of the families of periodic orbits involved in our study. Section 4 discusses the structure of the phase space when we perturb the initial conditions of our stable periodic orbits in the x-direction. We study successively the dynamical behavior close to the periodic orbit before (Sect. 4.1) and after (Sect. 4.2) the transition of the central family from stability to instability. We discuss as well the "rotation numbers" we define on the tori we have found (Sect. 4.3). Then, we increase the energy and we describe the changes we observe in the spaces of section in Sect. 4,4. The perturbations in the z-direction are presented in Sect. 5, which has a similar structure as Sect. 4. In Sect. 6 we vary the perturbation of our system. Finally in section 7 we discuss our results and we enumerate our conclusions.

2. The Hamiltonian System

The system we use for our applications rotates around its z-axis with angular velocity Ω_b . The Hamiltonian of the system in Cartesian coordinates is :

$$H(x,y,z,\dot{x},\dot{y},\dot{z}) = \frac{1}{2}(\dot{x}^2+\dot{y}^2+\dot{z}^2)+\Phi(x,y,z) -\frac{1}{2}\Omega_b^2(x^2+y^2) \quad (4)$$

where $\Phi(x,y,z)$ is the potential we used in our applications, i.e.:

$$\Phi(x,y,z) = -\frac{GM_1}{(x^2+\frac{y^2}{q_a^2}+[a_1+(\frac{z^2}{q_b^2}+b_1^2)^{1/2}]^2)^{1/2}} - \frac{GM_2}{(x^2+\frac{y^2}{q_a^2}+[a_2+(\frac{z^2}{q_b^2}+b_2^2)^{1/2}]^2)^{1/2}} \quad (5)$$

The potential in it's axisymmetric form ($q_a = 1, q_b = 1$) can de considered as a representation of the potential for the Milky Way approximated by two Miyamoto disks with masses M_1 and M_2 respectively (Miyamoto and Nagai 1975). In our units, distance R=1 corresponds to 1 kpc. For the Jacobi constant (hereafter called the "energy") Ej=1 corresponds to 43950 $(km/sec)^2$. We have used the following values for the parameters: $a_1 = 0\ kpc$, $b_1 = 0.495\ kpc$, $M_1 = 2.05 \times 10^{10}\ M_\odot$, $a_2 = 7.258\ kpc$, $b_2 = 0.520\ kpc$, $M_2 = 25.47 \times 10^{10}\ M_\odot$, $q_a = 1.2$, $q_b = 0.9$ and $\Omega_b = 60\ km\ s^{-1}\ kpc^{-1}$. The parameters q_a, q_b determine the geometry of the disks, while a, b are scaling factors (Binney & Tremaine 2008, p.73-74). The chosen Ω_b value puts corotation at R=4kpc and has been used by Englmaier and Gerhard (1999).

In Fig. 2 we give the (E_j, x) Zero Velocity Curve "ZVC" (see e.g. Contopoulos 2002 p.391). It refers to orbits on the equatorial plane z=0 and separates the regions where motion is allowed from those where it is forbidden.

3. The orbital evolution along a $S \rightarrow U$ transition

A method to follow the stability of a family of periodic orbits in a system is by means of the "stability diagram" (Contopoulos & Barbanis 1985; Pfenniger 1985a). The stability diagram gives the evolution of the stability of a family of periodic orbits in a system as one parameter varies, by means of the evolution of the stability indices b1, b2. In our case the parameter that varies is the energy Ej. Fig. 3 gives the evolution of the stability of the central family of periodic orbits in our system, x1 (Contopoulos and Papayannopoulos 1980), and its bifurcations at the interval $-5.5 <$Ej< -4.5. We observe that x1 (black lines for its indices b1 and b2) is initially stable and at Ej=-5.1644 it becomes simple unstable. There we have a $S \rightarrow U$ transition and a new family, x1v1 (red lines), is bifurcated and is stable. We call the

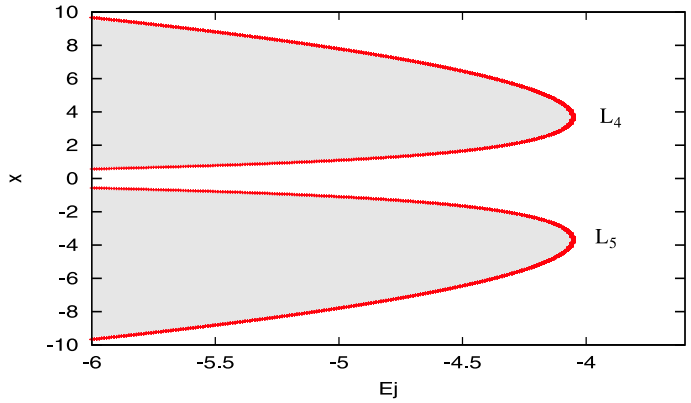

Fig. 2. The (Ej,x) Zero Velocity Curve (ZVC), for orbits on the z =0 plane, in our Hamiltonian system (4), with Φ as in (5) and parameter values given in the text. Motion is forbidden in the grey areas. L_4 and L_5 are the Lagrangian points on the minor axis of the galaxy.

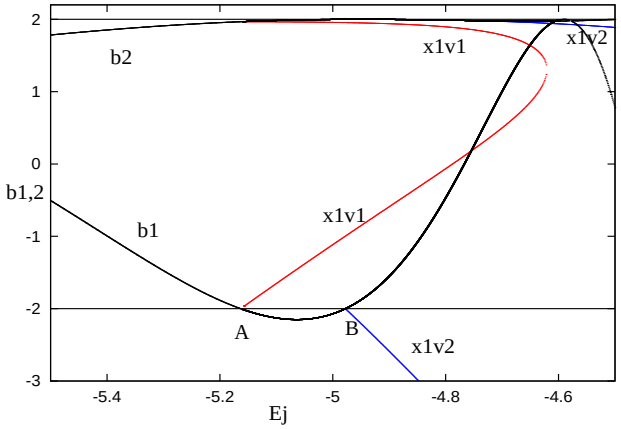

Fig. 3. Stability diagram for $-5.5 <$ Ej < -4.5, that shows the stability of the family x1 (black lines for its b1,b2 indices) and its bifurcating families of p.o. x1v1 (red) and x1v2 (blue). The two indices of the family x1v1 join at Ej=-4.62 and the family becomes complex unstable.

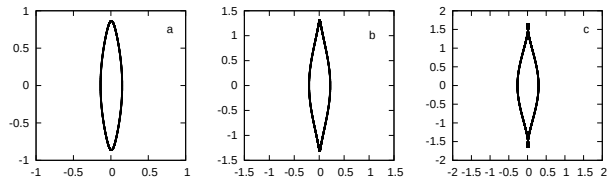

Fig. 4. Periodic orbits of x1 at a) Ej= −5.624726 (before "A"), b) Ej= −5.010526 (between "A" and "B") and c) Ej= −4.732626 (beyond "B").

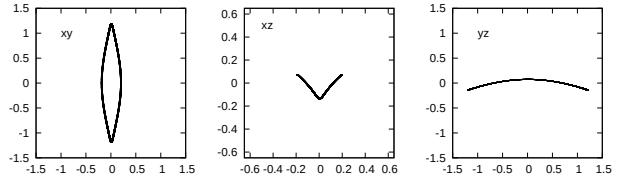

Fig. 5. A typical orbit of x1v1 at Ej = −5.125377 (between "A" and "B"). The (x, z) and (y, z) projections are given in enlarged scale, in order to better view the corresponding morphology.

transition point "A". The family x1 becomes stable again at Ej = −4.98, point "B", where we have an $U \rightarrow S$ transition for x1. At "B", is introduced the family x1v2 (blue line), which is initially simple unstable.

In Fig. 4 we present the morphological evolution of x1 as it appears before "A", between "A" and "B", and beyond "B". Point "A" is associated with the vertical 2/1 resonance (for a definition see e.g. Contopoulos 2002 p. 379). The importance of the 3D bifurcating family introduced at the vertical 2/1 resonance for the structure of galactic disks has been underlined in several studies (Pfenniger 1985b; Patsis and Grosbøl 1996; Skokos et al 2002a,b; Patsis et al 2002). Here we adopt the nomenclature of Skokos et al 2002a,b and we call the bifurcating families at Ej = −5.1644 and Ej = −4.98 x1v1 and x1v2 respectively. In Fig. 5 we give the morphology of x1v1 in a typical orbit at energies between "A" and "B".

4. Perturbations parallel to the equatorial plane

4.1. *Spaces of section before the $S \rightarrow U$ transition*

First we examine the surfaces of section for our system at energies before "A". Figs. 6a and 6b describe the surface of section for Ej=−5.207 (before "A"). Despite the fact that the system we investigate is of galactic type, the main goal of the present study is to understand the structure of the phase space in various cases in a 3D autonomous Hamiltonian system. In that sense we integrate our orbits for times necessary to obtain a clear view of the dynamical phenomenon we study, regardless of the physical meaning of the integration time interval, which can be more than a Hubble time. In Fig. 6a we observe the invariant curves around periodic orbits of two 2D families located on the equatorial plane z=0, in the $(x, \dot{x})$ space with initial conditions $(x_0 + \Delta x_0, \dot{x}_0, z_0, \dot{z}_0) = (0.18312784 + \Delta x_0, 0, 0, 0)$ with $\Delta x_0 = 0.1, \ldots, 0.8$ and $(x_0 + \Delta x_0, \dot{x}_0, z_0, \dot{z}_0) = (-0.59595941 + \Delta x, 0, 0, 0)$ with $\Delta x_0 = 0.1, \ldots, 0.4$. Every invariant curve consists of 10^3 consequents. The diagram describes a typical situation in rotating galactic potentials. The stable periodic orbit for $x > 0$ belongs to x1 (initial conditions $(x_0, \dot{x}_0, z_0, \dot{z}_0) = (0.18312784, 0, 0, 0)$) and the stable periodic for $x < 0$ to the retrograde family x4 (see Contopoulos 2002, p.391), which has initial conditions $(x_0, \dot{x}_0, z_0, \dot{z}_0) = (-0.59595941, 0, 0, 0)$. The extent of the invariant curves is limited by the ZVC. Varying the initial condition x_0 above the upper and below the lower limit of the ZVC at this Ej, always considering the plane of section $y = 0$ (cf. Fig. 2), we find the expected bell-type curves (10^3 points in the surface of section), which are related with escape orbits, as found by Contopoulos & Patsis (2006) (Fig. 6b).

4.2. *Spaces of section after the $S \rightarrow U$ transition*

Proceeding beyond "A", between "A" and "B", e.g. at Ej=−5.1574, we encounter, always for the surface of section $y = 0$, $\dot{y} > 0$, two simple periodic orbits with positive x_0. They are x1 (U), with initial conditions $(x_0, \dot{x}_0, z, \dot{z}_0)$ =(0.18958522, 0, 0, 0) and x1v1 (S), with initial conditions $(x_0, \dot{x}_0, z_0, \dot{z}_0) = (0.18939859, 0, 0.030236585, 0)$. We investigate the phase space structure close to these two periodic orbits, firstly by perturbing only the x initial conditions of x1 and x1v1 by $\Delta x = 0.1, 0.2 \ldots 0.7$ successively. The 2D simple unstable periodic orbit x1 lies on the equatorial (x, y) plane of our galactic model. By perturbing the initial conditions only in x and keeping the rest equal to 0, we encounter non-periodic orbits that remain on the (x, y) plane. Nevertheless, the surface of section of our 3D autonomous Hamiltonian system is 4D, $(x_0, \dot{x}_0, z_0, \dot{z}_0)$, and we can consider the $(x, \dot{x}, z)$ projection. For

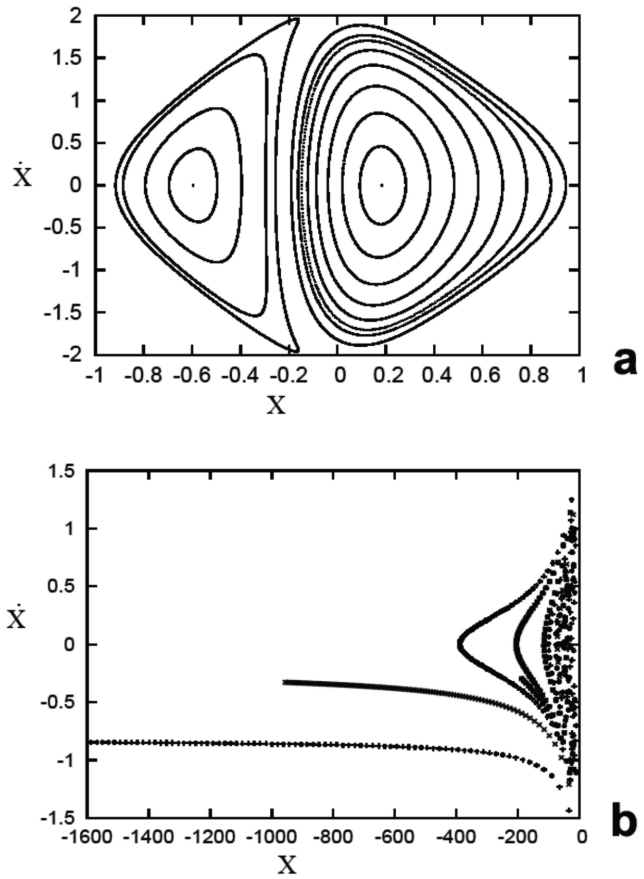

Fig. 6. The $(x, \dot{x})$ surface of section for Ej=−5.207. (a) The invariant curves are around the p.o. x1 (positive x) and x4 (negative x). (b) The surface of section considering initial conditions with x above the upper and below the lower limit of the ZVC at this Ej. We observe the appearance of "bell-type" curves (Contopoulos & Patsis 2006).

the simple unstable (U) periodic orbit x1, we have $z = 0$ always, thus the $(x, \dot{x}, z)$ is identical with the $(x, \dot{x})$ projection. This projection can be observed in Fig. 7, where we have seven invariant curves, surrounding the fixed point with the initial conditions of x1. Each invariant curve has about 10^3 consequents. We name these curves $S_{1a}, S_{2a}, \ldots, S_{7a}$ for the $(x_0 + \Delta x_0)$ perturbation of the x_0 initial condition with $\Delta x_0 = 0.1, 0.2, \ldots 0.7$ respectively.

In a way this is a counterintuitive result, since at this Ej x1 is characterized as simple *unstable*[2], having two of its eigenvalues on the real axis. We have also calculated the Lyapunov Characteristic Number (LCN) and we found it positive, equal to 0.025958. The Lyapunov Characteristic Number (LCN)[3] of the periodic orbits is defined as the maximum σ_i, where: $\sigma_i = \frac{1}{\tau}\ln(|\lambda_i|)$, τ is the period of the periodic orbit and λ_i the eigenvalues of the monodromy matrix of the Poincaré map (e.g. Lichtenberg and Lieberman 1992 p.302, Skokos 2010). Figure 7, underlines the fact, that the dynamical behavior close to a simple unstable orbit in a 3D Hamiltonian system can be similar to that at the neighborhood of a stable periodic orbit if the perturbation is restricted in one direction (in our case it is the radial one).

Applying the same seven perturbations to the x_0 initial conditions of x1v1 we encounter in the $(x, \dot{x}, z)$ space seven tori. The projection of the figure is given in Fig. 8. For this projection we use the point of view which is determined in spherical coordinates by the angles[4] $(\theta, \phi) = (17^o, 20^o)$ (see also introduction). We observe seven tori drawn with red color surrounding the x1v1 periodic orbit and we name them $S_1, S_2, S_3, S_4, S_5, S_6$ and S_7 starting with the closest to the periodic one. We also plot with green color the $S_{1a}, S_{2a}, S_{3a}, S_{4a}, S_{5a}, S_{6a}$ and S_{7a} invariant curves. Each torus consists of 10^4 consequents. Being just after the bifurcation point, the x initial conditions of x1 and x1v1 are almost identical. Thus, both the S_i tori and the S_{ia} invariant curves surround the "common" initial x value. On the $(x, \dot{x})$ projection the S_i tori and the S_{ia} invariant curves practically overlap.

The S_i tori are 3D projections of the invariant tori of our 4D Poincaré map. Their structure, except that of S_4, resembles the morphology of the objects defined as "rotational tori" by Vrahatis et al. (1996, 1997). These authors found the same kind of tori in a 4D symplectic map related with the problem of beam stability in circular particle accelerators. Even S_2, which seems to have its own internal structure (Fig. 8), becomes a typical rotational torus if we integrate for time giving 4×10^5 consequents (Fig. 9). An exception from this morphology is the torus S_4, which has a thin, complicated, ribbon-like structure. Fig. 10 presents S_4 in the 3D $(x, \dot{x}, z)$ space. The figure helps us understand that S_4 intersects itself at five places, namely A,B,C,D and E. In prac-

[2]Broucke (1969) characterizes this type of instability as "semi-instability", subdividing it to even- and odd- semi-instability, depending on whether the eigenvalues on the real axis are positive or negative respectively. In our case the eigenvalues are positive (even- semi-instability).

[3]When we use the term Lyapunov Characteristic Number we mean the maximal Lyapunov Characteristic Number.

[4]The $(0^o, 0^o)$ projection brings the x-axis and y-axis horizontally and vertically on the plane of the paper respectively and the z-axis perpendicular to them.

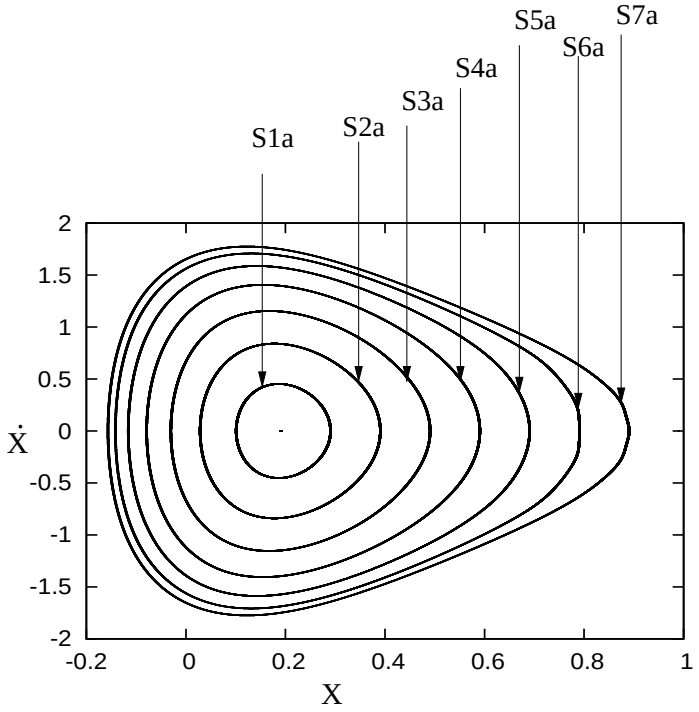

Fig. 7. The $(x, \dot{x})$ projection of the $(x, \dot{x}, z, \dot{z})$ cross-section space at the neighborhood of the 2D family x1 for $Ej = -5.1574$. The x1 periodic orbit at $(0.18958522, 0, 0, 0)$ is simple unstable. We name the invariant curves as $S_{1a}, S_{2a}, S_{3a}, S_{4a}, S_{5a}, S_{6a}, S_{7a}$ starting with the one closest to the periodic orbit.

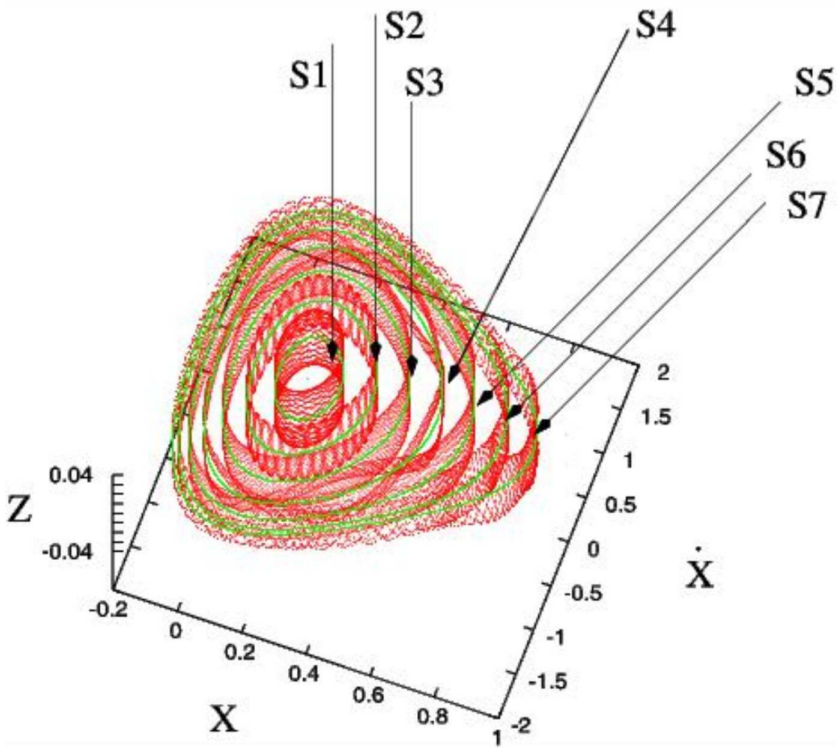

Fig. 8. The $(x, \dot{x}, z)$ 3D projection of the $(x, \dot{x}, z, \dot{z})$ 4D surface of section at Ej=−5.1574. Our point of view is $(\theta, \phi) = (17^o, 20^o)$. The S_i tori around x1v1 (see text) are drawn with red color, while the S_{ia} invariant curves around the x1 periodic are given with green lines.

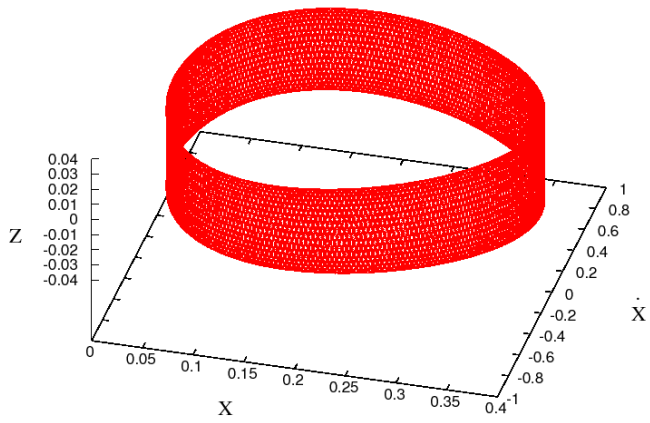

Fig. 9. The $(x, \dot{x}, z)$ projection of torus S_2 in the $(x, \dot{x}, z, \dot{z})$ 4D surface of section for Ej=−5.1574. Our point of view in spherical coordinates is now $(\theta, \phi) = (40^o, 15^o)$. This is a typical morphology of a 3D projection of a rotational torus.

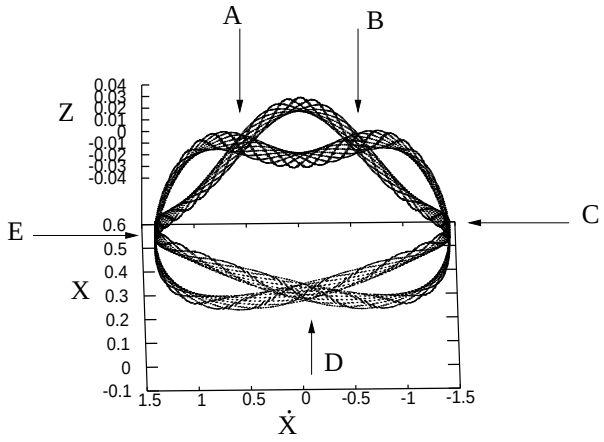

Fig. 10. 3D projection of torus S_4 from the point of view $(\theta, \phi) = (40^o, 264^o)$. A,B,C,D and E are the five intersections of S_4 by itself.

tice this can be realized only by rotating the figure on the screen of our computer to understand its detailed morphology. The structure of our S_4 tori resembles the morphology of the objects defined as "tube tori" again by Vrahatis et al. (1997).

Let us have now a closer look at the 4D structure of the rotational S_i tori by applying the method of color and rotation. The tori occupy a subspace of the 4D space of section bounded by $[x_1, x_2] \times [\dot{x}_1, \dot{x}_2] \times [z_1, z_2] \times [\dot{z}_1, \dot{z}_2] = [-0.154927, 0.890256] \times [-1.79387, 1.77590] \times [-0.0302, 0.0302] \times [-0.096, 0.096]$. As an example of the 4D structure of a rotational torus we depict in Fig. 11 the first 4×10^5 consequents of the S_2 torus. This torus has a small thickness, as it is generated by rotation around the $\dot{x}$-axis of a thin ellipse. We have chosen to plot the consequents in the $(\dot{x}, z, \dot{z})$ projection and color them according to their values in the x-dimension. With the help of a graphic software we have rotated S_2 in our computer screen in order to view it from all different perspectives and better understand its internal structure. We observed that there is no mixing of colors on the surface of S_2. On the contrary, we find that the color variation on it follows some rules. This property of the "rotational tori" was already known by Patsis & Zachilas (1994). However, the details, presented here for the first time, indicate a generic behavior that characterizes this class of objects.

Moving along the v-direction of the torus for constant u (see Fig. 1) the consequents keep their color by changing from the external to the internal side of the torus and vice versa when they reach certain four lines along the directions labeled with A, B, C and D in Fig. 11.

The details of the color variation close to these lines as we move along the v- direction for constant u, is shown in Fig. 12. This is an enlargement of the right part of Fig. 11, where e.g. red colored consequents on the external side of the torus change side sliding to the internal one, along the line indicated with "A" (upper left side in Fig. 12). If we continue moving clockwise on the v-direction the red consequents, now on the internal side of the torus, continue until we reach area "D". There, they change again side and turn to the external side. This allows us very clearly to observe the way that the transition from one side to the other happens. At the lower side of the figure we can observe how the red points slide behind the blue, forming a net. The "red net" is filled with red if we continue the calculation for longer time. Similarly the "blue net" on the inner side of the torus will be filled by blue after a long time and so do the red consequents at the lower left part of Fig. 12 will be covered by the blue. In our example we started moving along the v-direction from a red point. In general, the succession of colors in the v-direction with constant u angles can be understood by looking at the color-coded bar given at the right of the figures with the colored tori, e.g. in Fig.11. At the change of side of colors, red is combined with violet-blue (above or below it), orange with blue, yellow with light-blue etc. and finally at $u = 90^o$ and $u = 270^o$ the consequents have the shade of green (middle of the color-code bar).

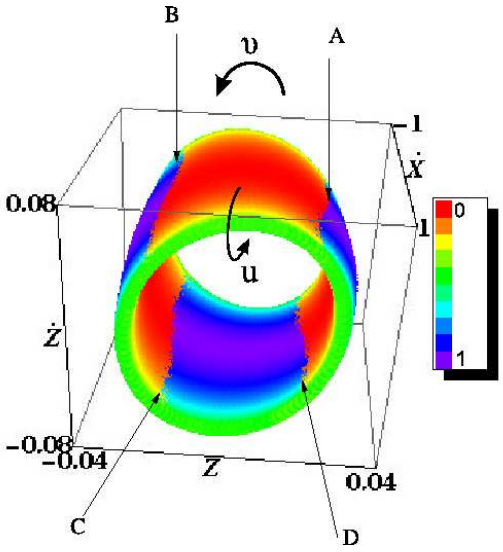

Fig. 11. The torus S_2 in the $(x, \dot{x}, z, \dot{z})$ 4D surface of section for Ej=−5.1574. The location of the consequents is given in the $(\dot{x}, z, \dot{z})$ projection and are colored according to their value in the x coordinate. Our point of view in spherical coordinates is $(\theta, \phi) = (180^o, 9^o)$.

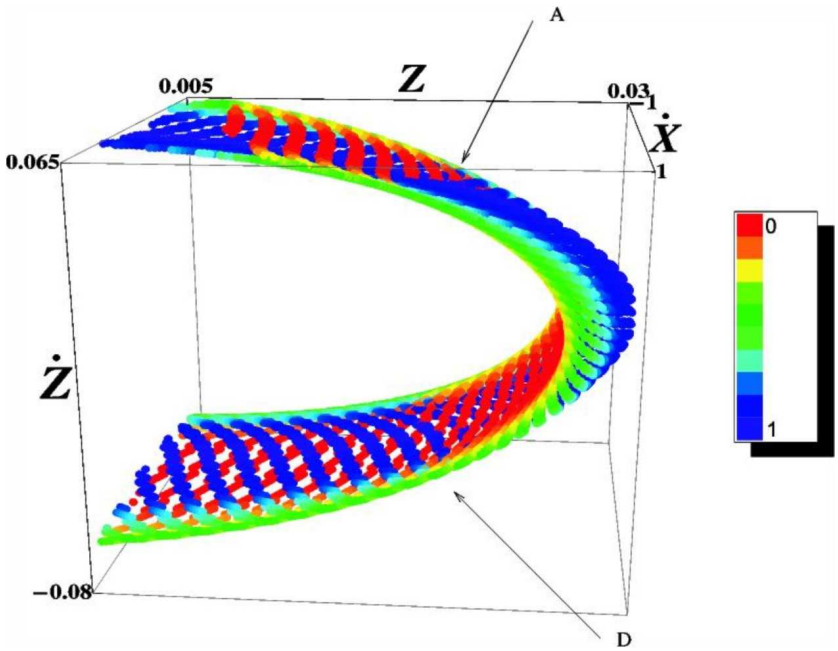

Fig. 12. The right part of the torus in Fig. 11 in enlargement. We observe how consequents of a certain color change from one side of the torus to the other.

Besides the color variation in the υ-direction, there is also color variation along u (constant υ). If we examine e.g. a "red-dominated" area on the S_2 torus in Fig. 11 we observe, that we get a red ($x = 0$) in the middle of the torus ($u = 0$). At first for $u : 0^o \to 90^o$ we observe a color variation from red to yellow and then to green, for values $\dot{x} = 0 \to 1$ (Fig. 11). Secondly for $u : 90^o \to 180^o$, at the internal side of the torus, the colors change from green to light blue, then to blue and finally to violet (now for values $\dot{x} = 1 \to 0$). Then, for $u : 180^o \to 270^o$ the colors change from violet to green (for values $\dot{x} = 0 \to -1$) and finally for $u : 270^o \to 360^o$, at the external side of the torus, we can observe a smooth color succession from green to yellow and then to red for values $\dot{x} = -1 \to 0$. In conclusion we observe

a cyclic variation of colors (values of x) along the u-direction. This means that the color variation is also smooth along $\dot{x}$, as described above. The color variation is similar for all rotational S_i tori.

In other cases of our system we find elliptic tori with considerable smaller ellipticity. We give an example not belonging to the $S \rightarrow U$ transition we use in our presentation. By perturbing the x initial condition of a stable periodic orbit with initial conditions $(x_0, \dot{x}_0, z, \dot{z}_0)$ =(0.6765982, 0, 0.254816, 0) for Ej=−4.3 (family x1v3, Skokos et al. 2002a,b) with $\Delta x = 10^{-5}$ we observe a torus which we name S_a (Fig. 13). In Figs. 13 and 14 torus S_a is depicted in the 3D subspace $(x, z, \dot{z})$ of the 4D surface of section and is colored according to the values of the 4th dimension $\dot{x}$. In Fig. 13 we observe that at the upper region of the external surface of the S_a dominate blue shades. Along the v-direction we observe a smooth color variation from blue to light blue, to green and to yellow. At a region indicated with an arrow labeled "A", we observe that yellow meets the blue. At this region we have an intersection of the external surface with the internal surface of the torus S_a. The details of the 4D structure of the torus close to the intersection is described in Fig. 14. The color continues from a yellow shade on the external surface (indicated with "Ext") of the torus S_a to orange and then to red on the internal surface of the torus (indicated with "Int" in Fig. 14). We observe a smooth variation of colors from red to the orange on the internal surface of the torus S_a (see also Fig. 13) until a region where orange meets the blue. At this region, indicated with arrow "B", we have in the 3D $(x, z, \dot{z})$ projection again an intersection of the external surface of the S_a with the internal surface of the torus S_a along a line.

We want to apply now the color and rotation method to the other kind of tori we found around x1v1 in Fig. 8. As we already remarked, S_4 has a different morphology than the rest of the S_i's, i.e. it is a tube torus. In the 3D projection $(x, \dot{x}, z)$ (Fig. 10) we have realized that S_4, intersects itself in five regions (A, B, C, D and E). In Fig. 15 the S_4 torus is colored according to the $\dot{z}$ values. In this figure we observe a smooth color variation at the areas between two successive intersections. For example we examine the area between the intersections A and B on the internal surface of the torus along the arrow "1". If we move from A as indicated with the arrow"1" (Fig. 15), for constant u, and starting with blue colored points, we can see a smooth color variation from blue to light blue, to green, to yellow, to orange at the intersection B. Now if we move from the intersection A along the direction indicated with the second arrow, "2" we have drawn at the "crossroad" A in Fig. 15, we observe that the succession of colors starting from red, at constant u, is red → orange → yellow → green → light blue → blue at the intersection B. In all cases we observe at the intersections of S_4 in the space $(x, \dot{x}, z)$ two different tubes, coming from different directions and having different colors. For example at the intersections A red meets blue and at the intersection B blue meets orange. Between two intersections of S_4 we observe a smooth color variation and in all cases at the intersections meet different colors. This means that the points have different values at the 4th dimension and the intersections are not intersections in the 4D space but only in the 3D projections.

4.3. *Rotation Numbers*

A point that we want to investigate, is whether some properties of the rotational and tube tori are reflected in quantities, that could be defined in correspondence with the rotation numbers on the usual invariant curves around stable periodic orbits of 2D systems. Thus we have first to define a rotation number in the 2D and 3D projections of a 4D torus. If our 4D space of section is $(x, z, \dot{x}, \dot{z})$, with the p.o. at $(x_0,z_0,\dot{x}_0,\dot{z}_0)$ we can consider e.g. its 2D projection in (x,$\dot{\text{x}}$) and its 3D projection in $(x, \dot{x}, z)$. Our motivation for this is the observation, that successive consequents form an invariant torus by filling its surface in different ways. Following the formation of an invariant torus on a screen as the number of consequents increases, one gets the impression that wires are wrapped around the surface of the torus, following different patterns for different tori. This seems to be a straightforward counterpart of the different angles at which an invariant curve is filled by successive consequents in 2D systems, which is described by the "rotation number" of an invariant curve. We want to attribute a similar number to each invariant torus. Let us assume that the projection of the torus on the $(x, \dot{x})$ plane gives an "invariant curve", in the same way that the S_i tori appear projected in Fig. 7. In such a diagram the rotation number (rot) is defined as for a usual invariant curve around a stable periodic orbit at $(x_0,\dot{x_0})$ on a 2D surface of section. In fact "rot" is the average rotation angle along the invariant curve. This quantity is different for different invariant curves and the variation of the rotation number as a function of the

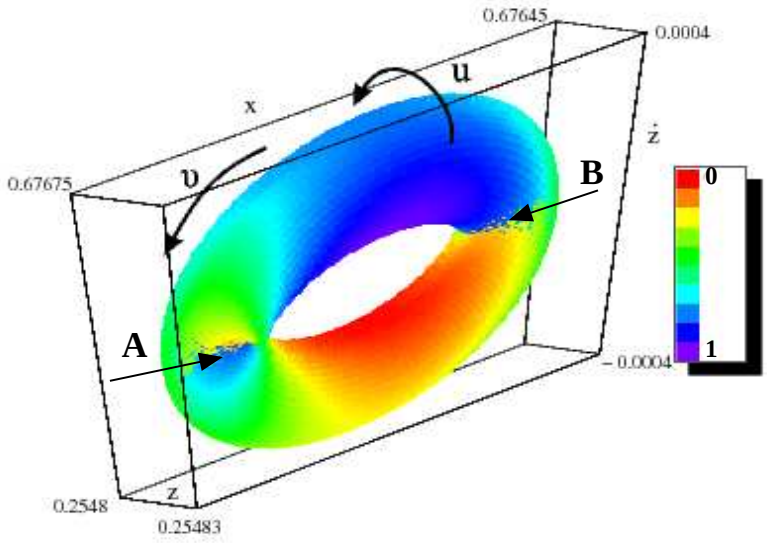

Fig. 13. The torus S_a around a stable p.o. x1v3 in the $(x, \dot{x}, z, \dot{z})$ surface of section for Ej=−4.3. The consequents are colored according to their value in the $\dot{x}$ coordinate. Our point of view in spherical coordinates is $(\theta, \phi) = (30^o, 30^o)$. We observe again a smooth color variation on the surface of the torus. The color changes side along the lines indicated with arrows.

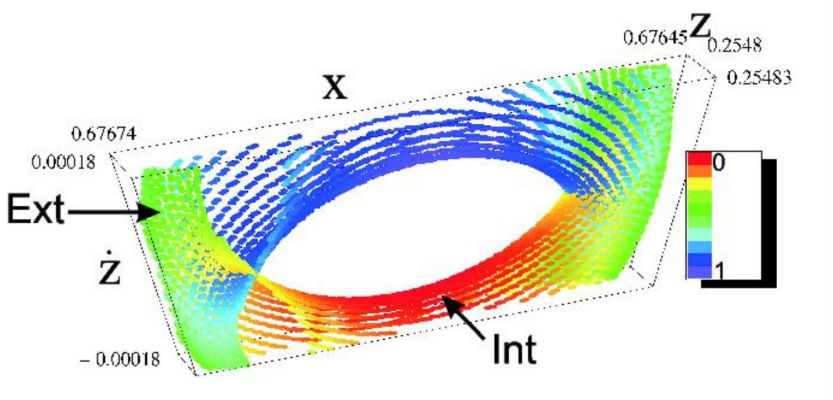

Fig. 14. The region of the intersection of the external surface with the internal surface of the torus S_a in the $(x, \dot{x}, z, \dot{z})$ 4D surface of section for Ej=−4.3. The consequents are colored according to their value in the $\dot{x}$ coordinate. Our point of view in spherical coordinates is $(\theta, \phi) = (30^o, 30^o)$. Arrows indicate the external and internal sides of the torus.

distance in the direction of a coordinate, e.g. the x-coordinate, defines a "rotation" curve (Contopoulos 2002, pg. 139).

Accordingly, for the calculation of *rot* for the torus in the $(x, z, \dot{x})$ projection,

(1) we define an initial rotation angle $\hat{r}_0$ for the initial point of an orbit on the invariant torus with coordinates $(x_1, \dot{x}_1, z_1)$ as the angle formed by the vector joining this point with the central periodic orbit $(x_0, \dot{x}_0, z_0)$ with the plane $(x, \dot{x})$. More precisely:

$$\hat{r}_0 = \arctan \frac{z_1 - z_0}{\sqrt{(x_1 - x_0)^2 + (\dot{x}_1 - \dot{x}_0)^2}} \qquad (6)$$

(2) We compute the rotation angle $\hat{r}_i$ between two successive consequents. The *i-th* consequent with coordinates $(x_i, \dot{x}_i, z_i)$ and the *i+1-th* with coordinates $(x_{i+1}, \dot{x}_{i+1}, z_{i+1})$ on an invariant torus. We define the vectors $\mathbf{X}$ and $\mathbf{Y}$ as $\mathbf{X} = (x_{i+1} - x_0, \dot{x}_{i+1} - \dot{x}_0, z_{i+1} - z_0)$ and $\mathbf{Y} = (x_i - x_0, \dot{x}_i - \dot{x}_0, z_i - z_0)$. respectively We find the rotation angle from the inner product of $\mathbf{X}$ and $\mathbf{Y}$ by means of the formula:

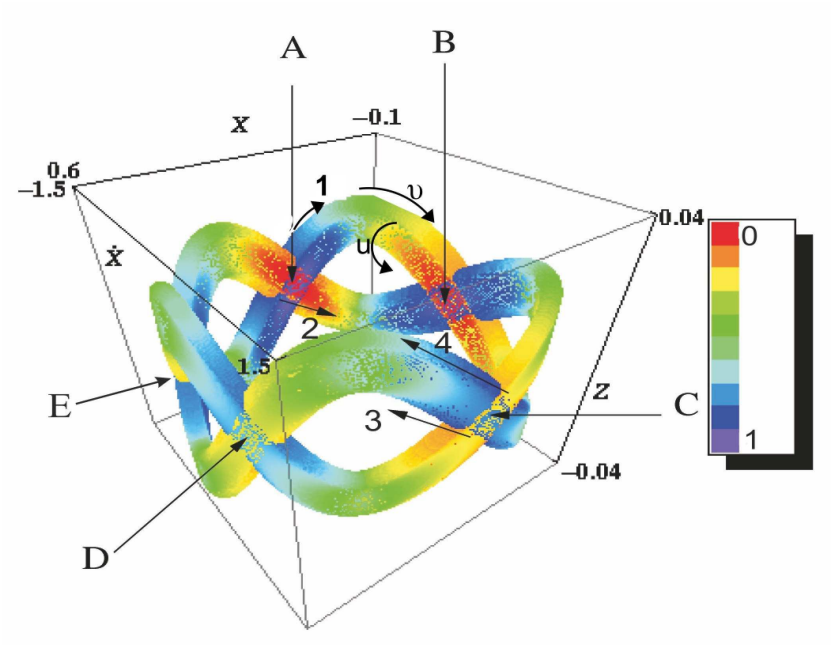

Fig. 15. The $(x, \dot{x}, z, \dot{z})$ 4D surface of section of torus S_4 for Ej=−5.1574. The consequents are colored according to their value in the $\dot{z}$ coordinate. Our view angles are $(\theta, \phi) = (30^o, 45^o)$.

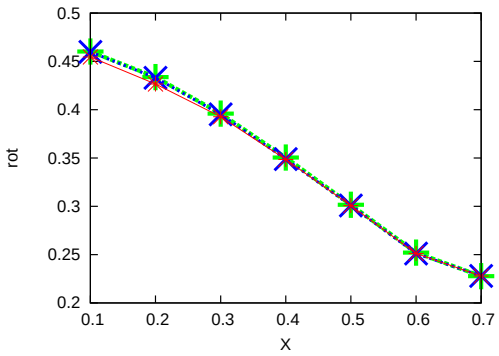

Fig. 16. Rotation curves at $Ej = -5.1574$ for the invariant curves around the periodic orbit of the x1 in the 2D subspace $(x, \dot{x})$ (green line), around the periodic orbit of the x1v1 in the 2D subspace $(x, \dot{x})$ (blue line), and around the periodic orbit of the x1v1 in the 3D subspace $(x, \dot{x}, z)$ (red line). We observe that the three curves have a very similar variation, and practically overlap.

$$\hat{r}_i = \arccos \frac{\mathbf{XY}}{\mid \mathbf{X} \mid\mid \mathbf{Y} \mid} \qquad (7)$$

(3) we finally compute the average of all $\hat{r}_i$'s to get *rot* for the torus.

The rotation curves along the x-direction, for the invariant curves around the simple unstable periodic orbit of the x1 family at Ej=−5.1574, with initial conditions $(x_0,z_0,\dot{x}_0,\dot{z}_0)$ $= (0.189585220, 0, 0, 0)$, is given in Fig. 16 (green curve). Notice that x1 is stable as regards deviations on the plane of symmetry, thus we can define a rotation number for orbits close to x1, starting on this plane. On the x-axis of Fig. 16 we give the distance from the periodic orbit in the x-direction. Similar curves are calculated for the tori around the stable periodic orbit of the x1v1 family at the same energy (Ej = −5.1574), which has initial conditions $(x_0,z_0,\dot{x}_0,\dot{z}_0)$= $(0.18939859, 0.030236585, 0, 0)$. Two rotation curves for x1v1 are given also in Figs. 16 using the $(x, \dot{x})$ (blue line) and $(x, \dot{x}, z)$ (red line) projections respectively. For the calculation of the rotation numbers in these rotation curves we followed the definitions mentioned above. We observe that in all cases we have a similar variation of the

rotation numbers. The behavior of rotation curves for the invariant tori around the stable periodic orbit of the x1v1 family has similar behavior with the rotation curve for the invariant curves around the simple unstable periodic orbit of the x1 family. We realize that the rotation numbers of the tube tori, follow the rotation curve and occupy the expected position in this diagram without any kind of exceptional behavior.

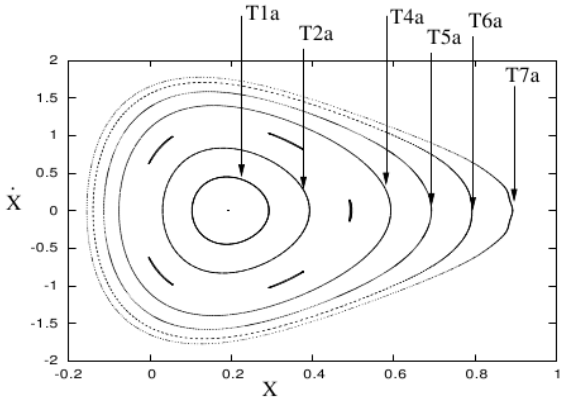

Fig. 17. The invariant curves $T_{1a}, T_{2a}, T_{4a}, T_{5a}, T_{6a}$ and T_{7a} in the $(x, \dot{x})$ surface of section for Ej=−5.131377.

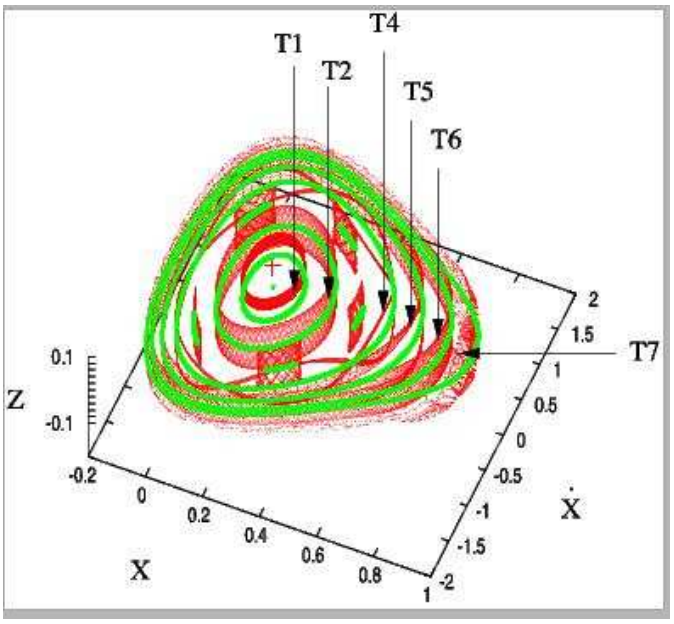

Fig. 18. The 3D $(x, z, \dot{x})$ projection of the 4D surface of section for Ej=−5.131377. Our point of view in spherical coordinates is $(\theta, \phi) = (18^o, 23^o)$. The invariant tori around the initial condition of the stable p.o. x1v1 are colored red and the invariant curves around the simple unstable p.o. of x1 on the $z = 0$ plane are colored green. The initial conditions of $x1$ and $x1v1$ are given with green and red crosses respectively.

4.4. *Energy variation*

Coming back to the evolution of the stability of the families x1 and x1v1, as described in Fig.3, we study the changes introduced in the structure of the phase space as the energy increases. At the bifurcating point the initial conditions of the families x1 (parent family) and x1v1 (bifurcating family) are identical. The x1v1 family comes in the system with two representatives at each energy (Skokos et al. 2002a). As Ej increases, we have one branch with $z > 0$ and the other one symmetric with $z < 0$. Let us consider here the $z > 0$ case. Close to the bifurcating point, the x_0 initial condition of the stable x1v1 orbit remain close to the $z = 0$ plane. Around the fixed point we find tori, which are practically symmetric with respect to the $z = 0$ plane. Away from the bifurcating point, for larger values of the energy, the value z_0 in the initial conditions of of x1v1 increases. Thus, beyond a given energy, in the $(x, \dot{x}, z)$ projection, the x_0 initial value of the simple unstable periodic orbit x1 is expected to be away from the tori around the stable periodic orbit x1v1, since these tori surround the x1v1 initial condition away from the z=0 plane. Here we study as an example the case for Ej= −5.131377, where the initial conditions of the simple unstable periodic orbit x1 are $(x_0, \dot{x}_0, z_0, \dot{z}_0) = (0.19317510, 0, 0, 0)$, while these of x1v1 are $(x_0, \dot{x}_0, z_0, \dot{z}_0) = (0.19221178, 0, 0.06769306, 0)$. Firstly we explore the phase space around the periodic orbit x1, which, also at this energy, is simple unstable. We do this by increasing the x_0 initial condition by $\Delta x_0 = 0.1, 0.2, 0.3, ..., 0.7$ and considering the $(x, \dot{x})$ surface of section (Fig. 17). The new element in Fig. 17 with respect to the $(x, \dot{x})$ phase space structure at $E_j = -5.1574$ (Fig. 7) is the appearance of a chain of 5 islands of stability at the location of the third invariant curve. These islands correspond to the orbit with initial conditions $(x_0 + 0.3, 0, 0, 0)$. Thus, one of the seven invariant curves of Fig. 7 has been broken as a result of the increase of Ej. We name the rest of the invariant curves $T_{1a}, T_{2a}, T_{4a}, T_{5a}, T_{6a}, T_{7a}$, with T_{1a} being the closest to the initial conditions of x1.

As in the previous case we investigate the neighborhood of the phase space around the 3D stable x1v1 by applying the same perturbations.

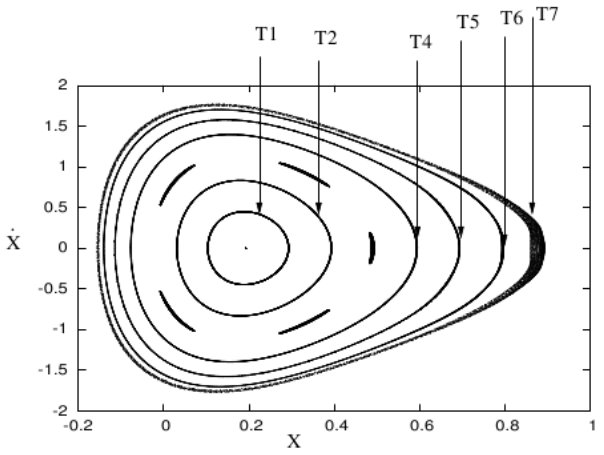

Fig. 19. The $(x, \dot{x})$ cross-section space at the neighborhood of the 3D family x1v1 for Ej=−5.131377.

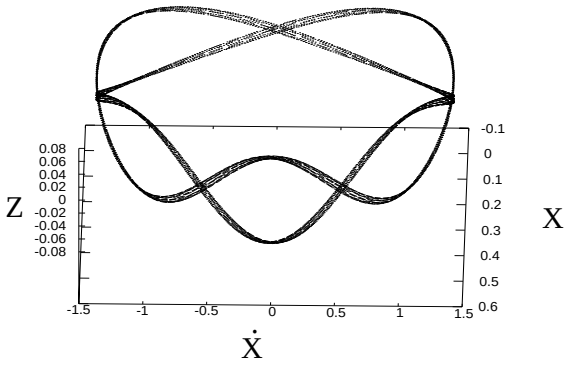

Fig. 20. The $(x, \dot{x}, z)$ 3D projection of the torus T_4 from the point view $(\theta, \phi) = (41^o, 91^o)$ we consider 10^5 consequents.

That means we increase the x_0 initial condition of x1v1 by $\Delta x_0 = 0.1, 0.2, \ldots 0.7$ and we consider the distribution of the consequents in the $(x, \dot{x}, z)$ projection of the 4D space after 10^4 intersections with the y=0 plane. We can observe the result in Fig. 18. The red-colored invariant tori around the initial condition of the stable p.o. x1v1 (red cross at $(0.19221178, 0, 0.06769306)$) correspond to the seven perturbed initial conditions we study. As in the case of the perturbed orbits around x1, also for x1v1 the third set of initial conditions, i.e. the one with $\Delta x_0 = 0.3$, exhibits a conspicuously different dynamical behavior. It forms a set of five small invariant tori, in correspondence to the five islands of stability formed on the $(x, \dot{x})$ plane in the case

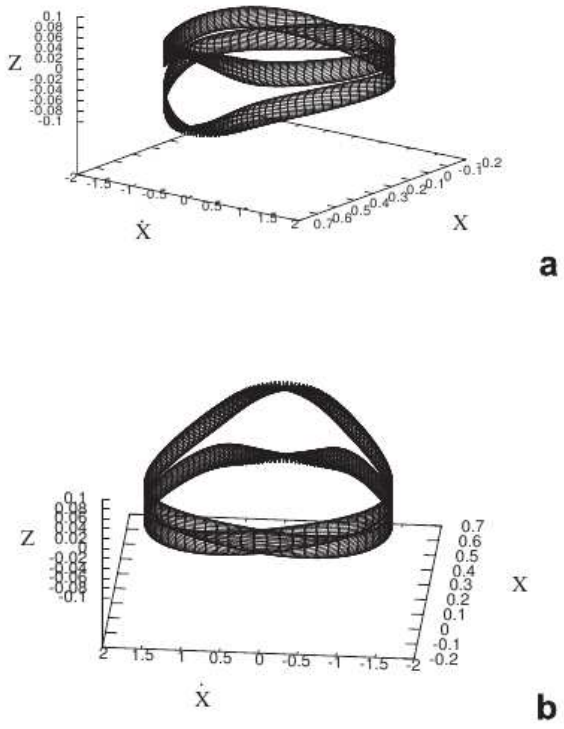

Fig. 21. 3D projections of torus T_5 from the point view $(\theta, \phi) = (64^o, 127^o)$ (a) and $(\theta, \phi) = (48^o, 271^o)$ (b).

of x1. Each one of the five small invariant tori has a rotational torus structure. We name the remaining six tori that surround the periodic orbit x1v1 as $T_1, T_2, T_4, T_5, T_6, T_7$. The missing T_3 has been substituted by the five small invariant tori. In Fig. 18 are given also the invariant curves around the p.o. of x1, colored green. They lie on the $(x, \dot{x})$ plane. We can observe that the tori are roughly projected on the $(x, \dot{x})$ plane in the region occupied by the green invariant curves. The projection of the 4D x1v1 surface of section to the $(x, \dot{x})$ plane is given in Fig.19. We observe that the 2D projection of the tori resembles the morphology of the invariant curves. Another interesting feature of the T_i invariant tori at the energy Ej= −5.131377 we study now, is that the T_4 torus to the right of the set of the 5 small ones, as well as the tori T_5 and T_7 are of different morphology than the rest of the T_i's.

In particular the torus T_4 (Fig. 18) has a thin, ribbon-like structure. Fig. 20 presents T_4 from a different point of view $((\theta, \phi) = (41^o, 91^o))$ in the $(x, \dot{x}, z)$ projection of the surface of section and helps us understand that T_4 indeed intersects itself in this projection at five places. The behavior of the T_4 is similar with the behavior of the S_4 torus

at the energy Ej=−5.1574 (Fig. 10).

T_5 has also a thin, complicated, ribbon-like structure (Fig. 21). This time the torus intersects itself only at one region in the $(x, \dot{x}, z)$ 3D projection as we can see in Fig. 21a and in Fig. 21b from different points of view of the $(x, \dot{x}, z)$ projection. Seven intersections in the $(x, \dot{x}, z)$ projection are also observed in T_7. T_4, T_5 and T_7 are objects that satisfy the definition of the tube tori given by Vrahatis et al. (1997).

As we said, in the $(x, \dot{x})$ projection the differences in the morphology of T_4, T_5 and T_7 from the rest T_i's cannot be seen (Fig. 19). Trying to understand if the difference we observe in the morphologies of the 3D projections of the tori reflect some morphological differences of the orbits in the configuration space we compare the orbits corresponding to the T_2 (rotational torus), with those of the tori T_4 and T_5 (tube tori) in Fig. 22. Their morphology is the expected for quasiperiodic orbits trapped close to a stable periodic orbit, in our case x1v1. The (x, y) projections of T_2, T_4 and T_5 are practically identical with the T_{2a},T_{4a} and T_{5a} orbits around x1 for the same Ej. There is no obvious morphological feature that distinguishes the three 3D orbits among themselves also in the (x, z) and (y, z) projections.

T_4 offers the opportunity to study in detail the structure of one more tube torus in the 4D space and compare it with the one depicted in Fig. 15, which we called S_4. Applying the color-rotation method also in this case, we observe, that the structure of T_4 (Fig. 23) is similar with that of S_4 (Fig. 15). We observe in Fig. 23, that moving along the tube from A towards B, following the directions indicated with arrows, we follow the succession of the colors of the color bar from one side to the other. At the intersection regions, in the $(x, \dot{x}, z)$ projection, the red color meets blue. This means that these regions are not intersections in the 4D space. Again here the intersections appear only at the 3D projections.

Different colors at the intersections characterize all tube tori we studied with the color-rotation method. A final example is given for the case of T_5. As we said before the torus T_5 is very thin, has almost a ribbon-like structure, and intersects itself at one region (Fig. 21). In Fig. 24 we depict a projection in the 3D subspace $(x, \dot{x}, z)$ and we color it according to the values of the consequents in the 4th dimension $\dot{z}$. By moving counterclockwise from the region A we observe again the smooth color variation. The colors change from green to light blue and then to blue until we reach the region C. At the region C T_5 intersects itself in the projection $(x, \dot{x}, z)$. Then, moving always counterclockwise, the succession of the colors continues as blue → light blue → green at the region B and finally comes back to the region C. At the region C we observe that blue color meets red. This means that the points have different values in the 4th dimension and C is not a region that we have a real intersection of T_5 in the 4D space. If we will continue our counterclockwise journey along the thin tubes of T_5 we will reach A following always a smooth color variation. Of special interest in this case is the folding of the thin, ribbon-like torus at the regions A and B. At these two regions the internal surface of the torus becomes external surface and vice-versa. This warping is encountered along the tubes of several other tori we studied. T_7 intersects itself in the 3D projections at 7 regions, while the tubes warp in the journey from one intersection to the other.

4.4.1. *Rotation numbers*

The rotation curves in the x-direction along the invariant curves around x1 and along the projected tori around x1v1 in the $(x, \dot{x})$ section, as well as the rotation curve from the tori around x1v1 in the $(x, \dot{x}, z)$ projection, calculated using the definition of Eq.(7), are very similar as in the case we presented above at Ej = −5.1574. Also here, at $E_J = -5.131377$, there is no special variation of the rotation curve at the locations of the tube tori. The variation of the rotation curves follows the general rules of these curves (see Contopoulos 2002). The main difference is that at the location of the stability islands around x1 and the tori-chains around x1v1 we find tiny plateaus on the rotation curve as expected.

5. Perturbations in the z- and ż-direction

The radial perturbations we studied until now, gave us an understanding of the structure of the tori in the neighborhood of stable periodic orbits in our galactic type Hamiltonian System. However, of particular interest is the evolution of the tori also under vertical perturbations. Especially in 3D galactic systems we want to know how, and in what extent, stars are trapped away from the equatorial plane. This study is related with the investigation of morphological features as boxy and peanut-shaped bulges in disk galaxies (Patsis et al. 2002).

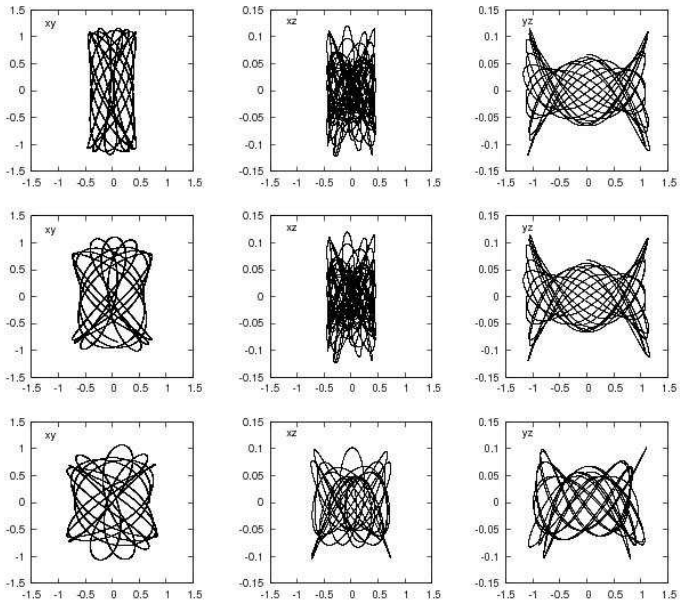

Fig. 22. The orbits in the configuration space corresponding to the tori T_2 (first row), T_4 (second row) and T_5 (third row). Projections are indicated at the upper left corner of each panel. In the (x, z) and (y, z) projections the scales on the axes are not equal, so that we can see the detailed of the orbits.

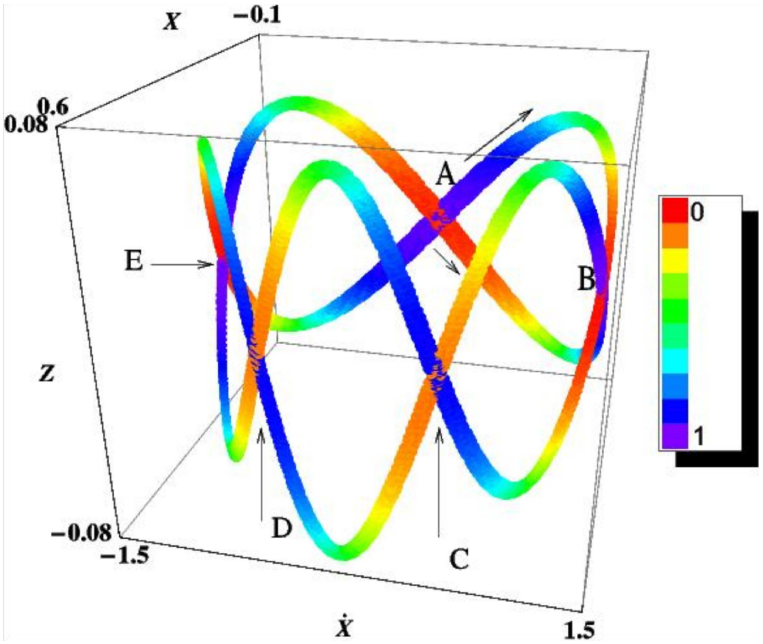

Fig. 23. The $(x, \dot{x}, z, \dot{z})$ 4D surface of section of the torus T_4 for Ej=−5.131377. The consequents are colored according to their value in the $\dot{z}$ coordinate. Our view angles are $(\theta, \phi) = (30^o, 120^o)$. The five intersections points of the tube torus by itself in the $(x, \dot{x}, z)$ are labeled with A,B,C,D and E.

5.1. *Spaces of section before the $S \rightarrow U$ transition*

Going back to the stability diagram given in Fig. 3, that describes the stability evolution of the families x1 and x1v1, we study first the phase space at an energy before the $S \rightarrow U$ transition, i.e. at Ej=−5.207. In this case, on the $(x, \dot{x})$ surface of section the only 2D simple periodic orbit we have with $x > 0$ is x1 and it is stable. Around x1, we find

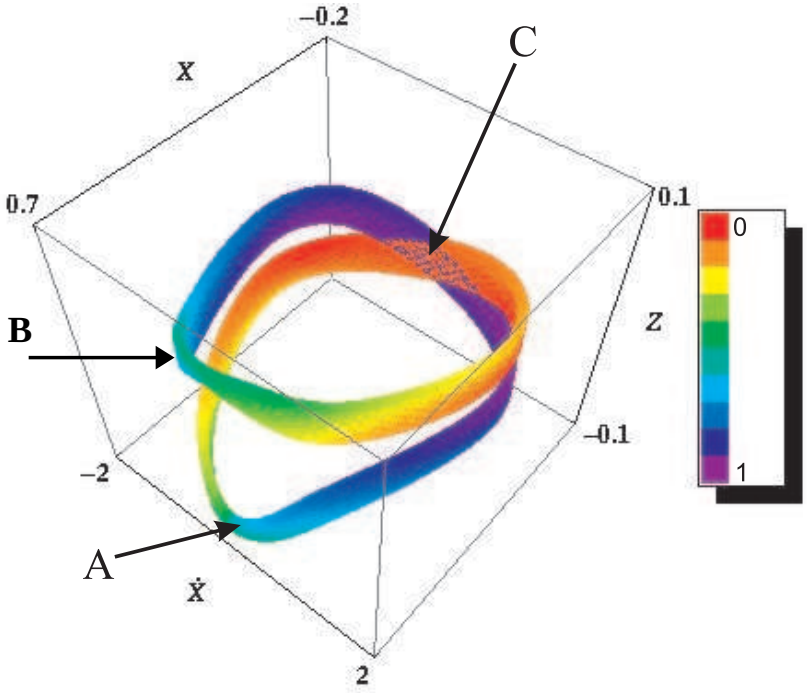

Fig. 24. The $(x, \dot{x}, z, \dot{z})$ 4D surface of section of torus T_5 for Ej=−5.131377. The consequents are colored according to their value in the $\dot{z}$ coordinate. Our view angles are $(\theta, \phi) = (30^o, 72^o)$.

invariant curves as expected, if we perturb its x_0 initial condition. As an example we consider the invariant curve, which results from the initial conditions $(x_0 + \Delta x_0, \dot{x}_0, z_0, \dot{z}_0) = (0.18312784 + \Delta x_0, 0, 0, 0)$, with Δx_0=0.1. If we "perturb" this quasi-periodic orbit, i.e. if we increase further the $z_0 = 0$ initial condition by Δz_0=0.1, 0.2 ..., and integrate again our initial conditions, we encounter tori around x1. These are both rotational and tube tori. The tori, for small Δz_0 surround the invariant curve we perturbed. For $\Delta z_0 \geq$0.3 the tori appear distorted and inclined with respect to the $z = 0$ plane. However, for Δz_0=0.41 the dynamical behavior at the neighborhood of the quasi-periodic orbit changes. About the first 900 consequents of this orbit form an object that resembles a rotational torus. By this we mean that initially the consequents stay approximately on a toroidal surface. However, the following consequents diffuse in the phase space and occupy a larger volume in it. In Fig. 25a we observe the $(x, \dot{x}, z)$ projection of the 4D surface of section for this orbit, where the 4th dimension is represented by the colors of the 4th $\dot{z}$ coordinate. The number of consequents in Fig. 25a is 1100. They form a (rotational) toroidal surface, with a smooth color variation around it as we can see by comparing the colors on its surface with the color bar to the right of the figure. We note, that 900 consequents do not suffice to fill densely the surface of the toroidal object. Thus, on Fig. 25a we observe distinct points rather than a toroidal object. However, starting e.g. from upper left, we observe the succession of colors from green → yellow → orange → red → orange → yellow → green → to blue shades. In Fig. 25a some points have already started deviating from the "torus" and soon they occupy a larger area of the phase space. In Fig. 25b, the dense cluster of red points corresponds to the 900 consequents we plotted colored in Fig. 25a. The rest of the red points that occupy a larger area of the phase space belong to the same orbit, which has been integrated now for 1.2×10^4 consequents. In the same figure we give as well the invariant curve around x1 at this energy, drawn with green color. This dynamical behavior indicates stickiness (Contopoulos & Harsoula 2008). Qualitatively, we find similar results if we increase $\dot{z}_0$ instead of z_0, in the initial conditions $(x_0, \dot{x}_0, z_0, \dot{z}_0) = (0.28312784, 0, 0, 0)$ following the procedure described above.

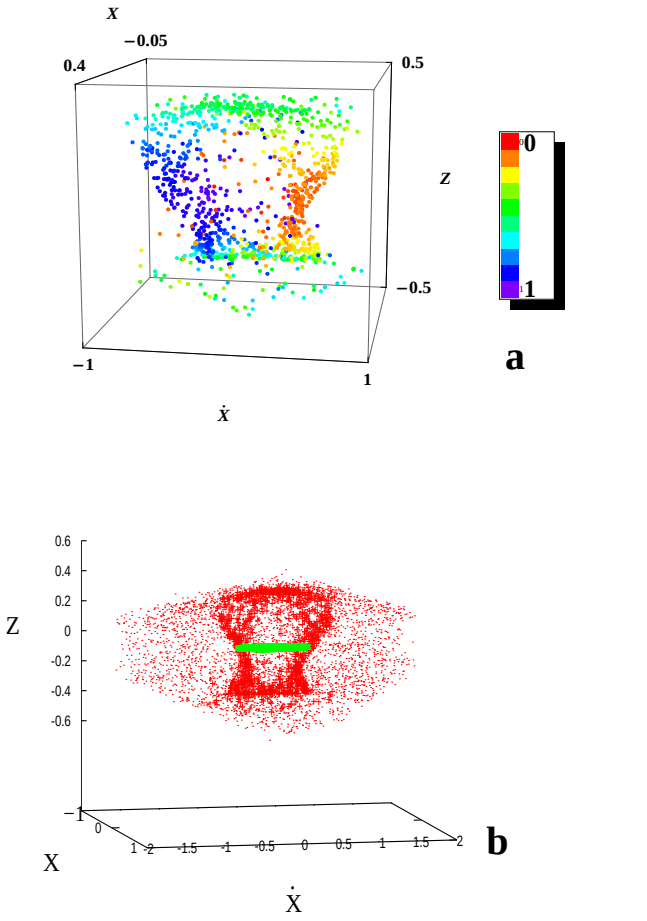

Fig. 25. The 3D $(x, z, \dot{x})$ projection of the 4D surface of section in the neighborhood of x1 for Ej=−5.207. The initial conditions of the orbit are $(x_0, \dot{x}_0, z_0, \dot{z}_0) = (0.28312784, 0, 0.41, 0)$ (see text). (a) the first 1100 consequents colored according to their position in the 4th dimension $\dot{z}$. The point of view is $(\theta, \phi) = (78^o, 82^o)$. (b) The first 1.2×10^4 consequents (red dots). The initial condition of x1 is indicated with a green dot, while the green invariant curve around it correspond to the orbit with initial conditions $(0.28312784, 0, 0, 0)$. The red points diffuse in the phase space after staying on a toroidal surface for about 900 consequents.

5.2. *Spaces of section after the $S \rightarrow U$ transition*

As we already have seen, after the $S \rightarrow U$ transition, x1 becomes simple unstable, while the 3D stable family x1v1 has been bifurcated. The energy Ej=−5.131377 is already beyond the bifurcating point (Fig. 3). We have examined the phase space structure in the neighborhood of x1 and x1v1 by perturbing their x_0 initial conditions and the result is depicted in Fig. 18. At energies not far away from the bifurcating point A (Fig. 3), as is Ej=−5.131377, we could always find a "$\pm\Delta z_0$" perturbation of the quasi-periodic orbits, so that the initial condition $(x_0 + \Delta x_0, 0, \pm\Delta z_0, 0)$ gives a torus surrounding the invariant curve $(x_0 + \Delta x_0, 0, 0, 0)$, with $(x_0, 0, 0, 0)$ being the initial condition of x1.

However, at larger energies this was not always possible. We could find invariant curves around x1, that deviate in the phase space from the invariant tori around x1v1 at the same energy. For example at Ej=−4.98996, we find invariant curves around x1 and invariant tori around x1v1 by perturbing the x_0 initial conditions of both families. In Fig. 26 we give in the 3D $(x, z, \dot{x})$ projection the invariant curves around x1 for $x_0 + \Delta x_0 = 0.1$, 0.2 and 0.3 (green curves) and the corresponding tori around x1v1 applying the same perturbation to its initial conditions. The invariant tori "float" above the invariant curves. We observe that as we depart from the x1v1 initial condition the invariant tori become thicker in z. Beyond a certain $x_0 + \Delta x_0$ perturbation there are invariant tori that intersect the $(x, \dot{x})$

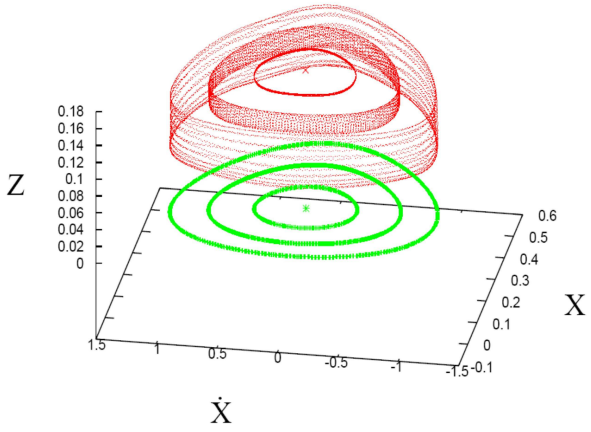

Fig. 26. The 3D $(x, z, \dot{x})$ projection of the 4D surface of section at Ej=−4.98996 for three invariant tori around $x1v1$ and three invariant curves around x1 (green lines). Our point of view is $(\theta, \phi) = (56^o, 280^o)$. The initial condition of $x1$ is indicated with a green star and the initial condition of $x1v1$ is given with a red "×".

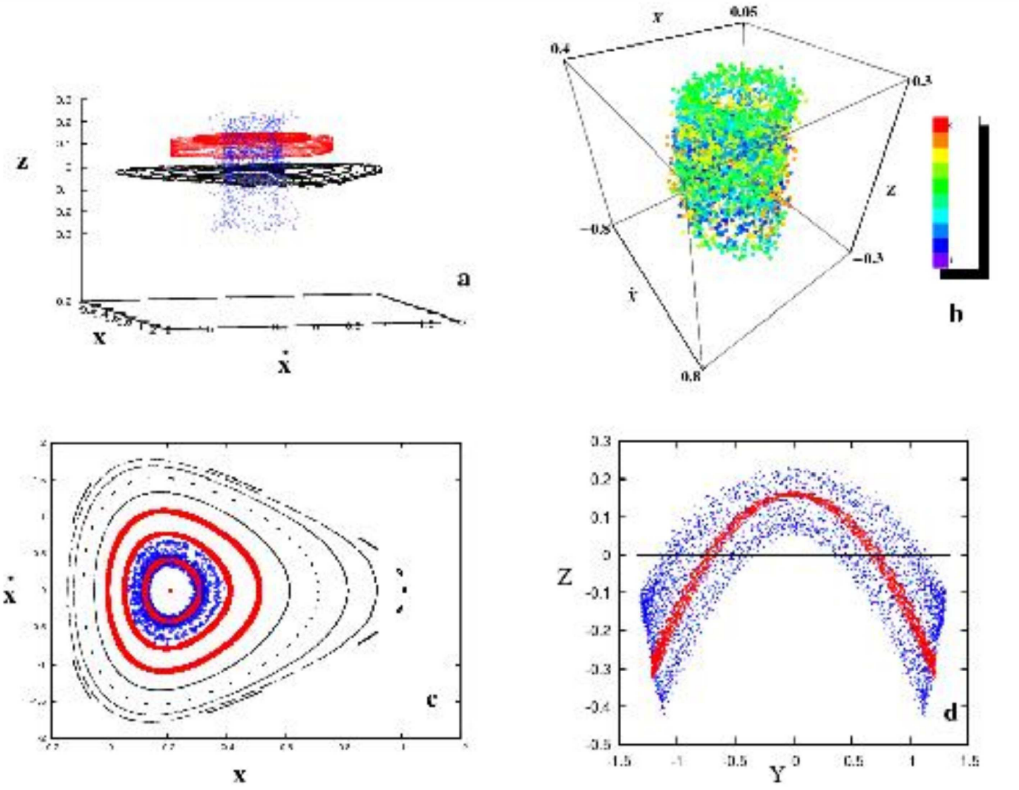

Fig. 27. (a) A chaotic orbit at Ej=−4.98996 in the 3D $(x, z, \dot{x})$ projection (point of view $(\theta, \phi) = (55^o, 263^o)$) of the 4D surface of section is given with blue dots. We also give three rotational tori around x1v1 (red), and seven invariant curves around x1 in the $(x, \dot{x})$ plane. (b) The 4D surface of section of the cloud of blue points we give in (a) (point of view $(\theta, \phi) = (60^o, 45^o)$). It is characterized by scattering of their colors in the 4th dimension. (c) The $(x, \dot{x})$ surface of section for the orbits in (a). We see that the blue points extend inside as well as outside the innermost rotational torus. (d) The chaotic orbit (blue points) together with the quasi-periodic x1v1 orbit corresponding to the innermost rotational torus in (a).

plane (not depicted in Fig. 26).

In the case depicted in Fig. 26 we successively "perturb" the initial conditions of the quasi-periodic orbits that correspond to the red invariant tori by $-\Delta z_0$ trying to find other invariant tori, that their projections in z reach the $(x, \dot{x})$ plane. Follow-

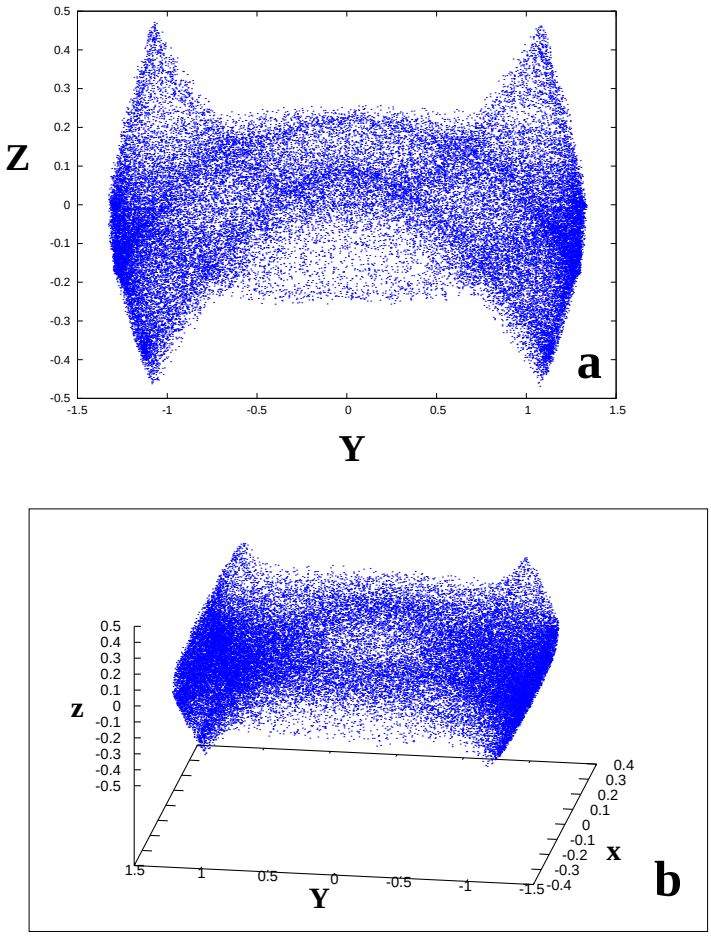

Fig. 28. (a) The (y, z) profile of the orbit corresponding to the cloud of blue points in Fig. 27a. (b) The same orbit in the configuration space from a point of view $(\theta, \phi) = (63^o, 280^o)$.

ing this procedure we find a last invariant torus with $(x_0 + 0.1, 0, z_0 + \Delta z_0, 0) = (0.3160689, 0, -0.08, 0)$, i.e. for $\Delta z_0 = -0.08$. For $\Delta z_0 = -0.09$ instead of a torus we find a cloud of points at the area between the invariant curves and the invariant tori. This cloud is given in Fig. 27a with 1.2×10^4 blue points, together with the three rotational tori around x1v1 depicted in Fig. 26 (colored red) and seven invariant curves around x1 on the $(x, \dot{x})$ plane (black curves). For about the first 3000 consequents, the cloud has a vague toroidal structure in the $(x, \dot{x}, z)$ projection. In Fig. 27b we apply the color-rotation method in the set of blue points of Fig. 27a, which we color according to their value in the $\dot{z}$ coordinate. It becomes clear that the points do not have a smooth variation in the 4th dimension. The same color mixing is also present in the figure with fewer consequents. Particularly helpful is the $(x, \dot{x})$ projection of Fig. 27a, given in Fig. 27c. In this projection we can clearly observe, that blue points of the cloud can be found inside, as well as outside of the red innermost invariant rotational torus. The vast majority of the points diffuses outside the the $(x, \dot{x})$ projection of that torus between 4×10^3 to 5×10^3 consequents, building a second ring at the outer side of the torus of lower intensity than the ring in its inner side. It is interesting to realize that such chaotic orbits may contribute to the thickening of observed structures as the peanut-shaped bulges of disk galaxies. The backbone of such peanut-shaped structures is the x1v1 family (Patsis et al. 2002). In Fig.27d the trapped quasi-periodic orbit around the stable p.o. x1v1 at this energy (Ej=−4.98996) is plotted with red dots, while the blue points give the chaotic orbit that we plot in Fig. 27b in the configuration space ((x, z) projection). The blue orbit in Fig.27 is integrated for a time corresponding to 0.2 Hubble times, i.e. in a time generally believed

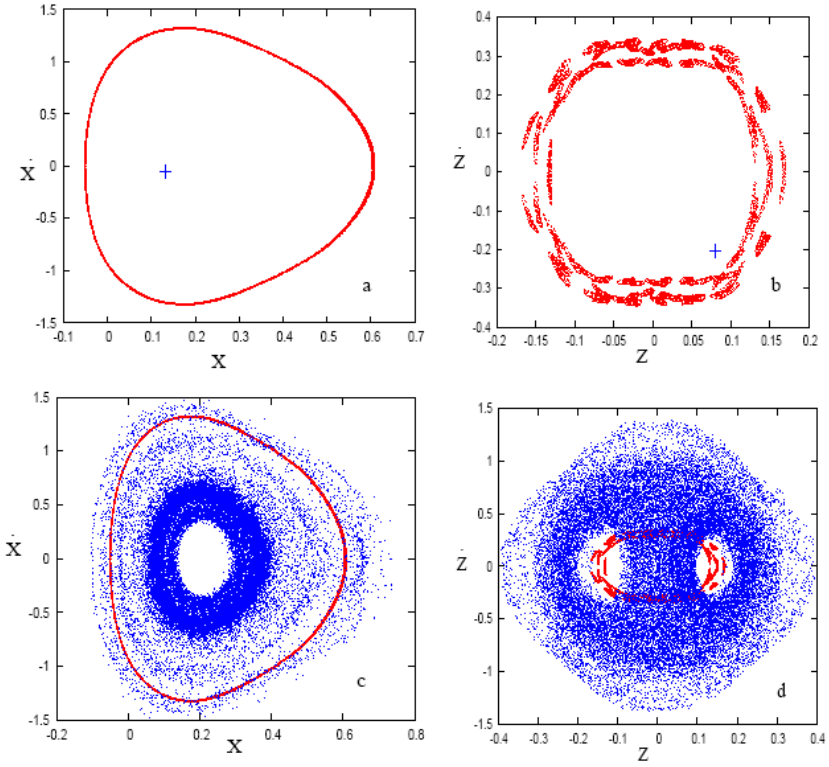

Fig. 29. The relative location of the consequents of the chaotic orbit of Fig. 28, with respect to the location of the tube torus "X4" (see text). In (a) and (b) we give with a blue cross, the location of a single consequent that it is projected in the interior of the $(x, \dot{x})$ and $(z, \dot{z})$ projections of "X4" respectively. In (c) and (d) we give all the 1.2×10^4 consequents of the orbit, clearly showing that we have points inside and outside "X4".

that morphological features as the galactic bars can well survive (see e.g. Debattista et al. 2006).

For longer times, of the order of 0.7 of a Hubble Time, the shape of the "blue" orbit still follows the peanut morphology, having populated both branches of the stable p.o. x1v1 (Patsis et al. 2002) at this energy. Thus, the peanut shape is fully developed, despite the fact that the orbit reaches z values 1.5 times larger than the quasi periodic orbit in the neighborhood of x1v1 (innermost rotational torus). In Fig. 28a we give the (y, z) projection for comparison with the models of periodic orbits in Patsis et al. (2002), while in Fig. 28b we give the same orbit from the point of view $((\theta, \phi) = (63^o, 280^o))$, so that it becomes clear the relation between the peanut side-on profile of the orbit and its "pencil-sharpener" 3D morphology. This class of orbits may be very important for the kinematics of peanut-shaped bulges of disk galaxies, as they increase the dispersion of the velocities of the stars, participating in this structure without destroying its morphological profile. These orbits are chaotic, but for times important for Galactic Dynamics have consequents that stay close to the invariant tori of x1v1 in the phase space. However, for larger times they diffuse away from the invariant tori in the phase space.

None of the blue consequents presented in the $(x, \dot{x})$ projection (Fig. 27c) inside the innermost red torus could be found projected simultaneously in the interior of the torus in the $(z, \dot{z})$ projection. However, this was not true for the location of consequents relative to tori at larger distances from the periodic orbits than the three rotational tori we considered in Figs. 26 and 27. An example is given for the torus we obtained by perturbing by Δx_0=0.4 the x1v1 initial conditions. This is a tube torus and let us call it "X4". In Fig. 29 we give with a blue cross the position of a consequent which is simultaneously projected in the interior of "X4" of the $(x, \dot{x})$ (Fig. 29a) as well as of the $(z, \dot{z})$ projection (Fig. 29b). It is one of the consequents depicted in Figs. 29c and Fig. 29d, where we clearly observe that we have consequents of the "blue" orbit inside and outside the tube torus "X4". This tells us that in this case takes place the phenomenon of Arnold diffusion (see e.g. Contopoulos 2002, pg.

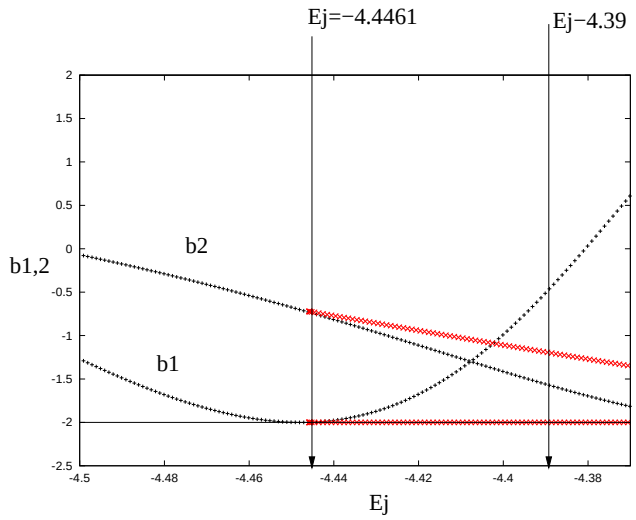

Fig. 30. Stability Diagram for −4.5 <Ej < −4.37, that gives the stability indices of the family x1 and its bifurcating family of p.o. x1v1, in the axisymmetric case of our model ($q_a = 1, q_b = 1$).

344). Nevertheless the time scale for this exceeds one Hubble Time. Thus, in this particular case the consequences for the dynamics in the neighborhood of x1v1 are negligible. However, in a forthcoming paper we investigate in detail this as well as other cases of Arnold diffusion in the Hamiltonian system of Eq. 4 and Eq. 5.

Before closing this section we want to underline that the same procedure can be repeated by perturbing the $\dot{z}_0$ initial condition, reaching the same results as regards the appearance and the foliation of the tori in the 4D space.

6. The evolution of the tube tori as the perturbation increases

Finally we examine the evolution of the invariant tori as the perturbation of our system increases, starting from the axisymmetric case ($q_a = 1$ and $q_b = 1$). In our model we increase the perturbation by increasing the triaxiality of the system through the parameters q_a and q_b. At first we examine the axisymmetric case and then we introduce a small perturbation ($q_a = 1.01$ and $q_b = 1$), in order to study possible qualitative differences that are introduced in the system by the perturbation.

6.1. *The Axisymmetric case ($q_a = 1, q_b = 1$)*

In 3D axisymmetric potentials the stability index of the central family, which is related with perturbations vertical to the equatorial plane, becomes tangent to the b=−2 axis at the vertical resonances (e.g. Patsis & Grosbøl 1996). Fig. 30 gives the evolution of the stability of the central family of periodic orbits of our system, x1, and its vertical bifurcation (x1v1) for −4.5 <Ej< −4.37. We observe that x1 (b1, b2 indices with black lines) is initially stable and at Ej=−4.4472 we have a tangency of b1 with the −2 axis. This tangency corresponds to the ver-

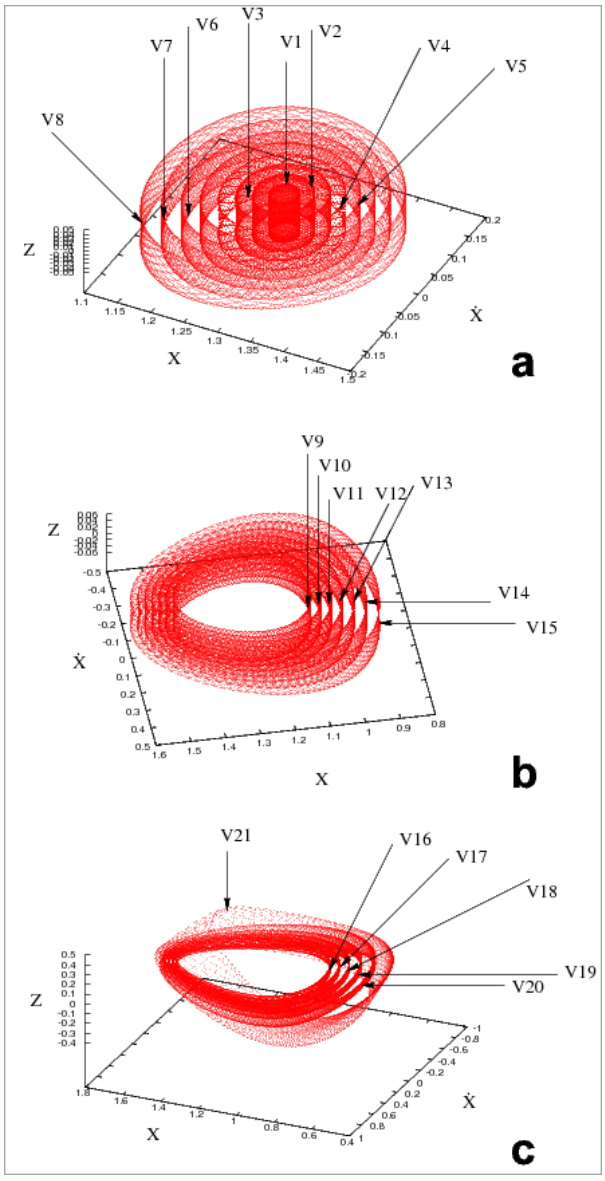

Fig. 31. $(x, \dot{x}, z)$ 3D projections of the 4D surface of section in the axisymmetric case, for Ej=−4.4461, at the neighborhood of the marginally stable p.o. x1v1. (a) The first 8 invariant tori V1...V8 (point of view $(\theta, \phi) = (38^o, 211^o)$). (b) The invariant tori V9...V15, (point of view $(\theta, \phi) = (36^o, 244^o)$). (c) The last six tori of our sample, V16...V21, (point of view $(\theta, \phi) = (49^o, 195^o)$). We observe the deformation of the last torus V21.

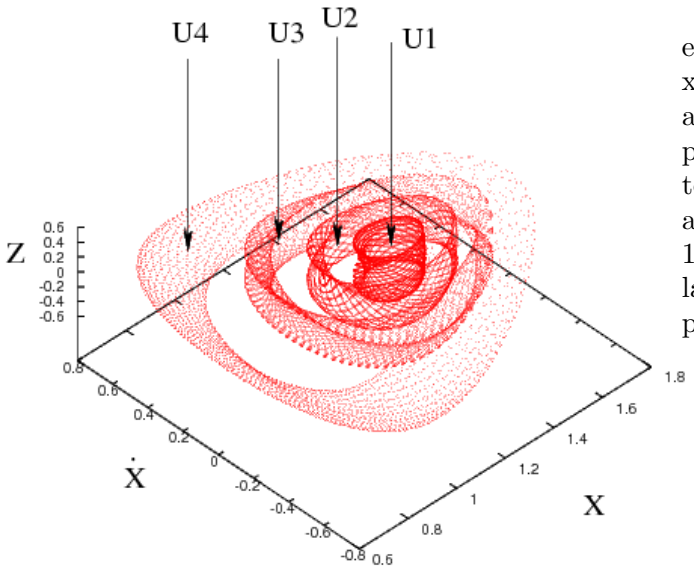

Fig. 32. The $(x, \dot{x}, z)$ 3D projection of the 4D surface of section in the neighborhood of the p.o. x1v1 for Ej=−4.39. Our point of view is $(\theta, \phi) = (27^o, 316^o)$.

tical 2/1 resonance. At this point it is bifurcated a new family (x1v1) (the two stability indices of x1v1 are drawn with red lines), which remains marginally stable, since we find that one of its stability indices stays on the −2 axis.

We have taken several surfaces of section and we studied the structure of the phase space at the neighborhood of the marginally stable p.o. x1v1. We first studied the phase space structure close to x1v1 for Ej=−4.4461, just after the tangency of the b1 index with the b=−2 axis. We integrated 21 initial conditions at the neighborhood of x1v1 $(x_0, z_0, \dot{x_0}, \dot{z_0}) \approx (1.298965, 0.041883918, -.0036186582, 0.026639957)$, by perturbing the x_0 initial condition of x1v1 by $\Delta x_0 = 0.02, 0.04 \ldots 0.42$ successively. Fig. 31 gives the $(x, \dot{x}, z)$ 3D projections of the tori we found around x1v1. In Fig. 31a we observe the first eight rotational tori $V_1, V_2, \ldots V_8$ and in Fig. 31b the rotational tori $V_9 \ldots V_{15}$. Finally in 31c we give the last six tori $V_{16} \ldots V_{20}$ and V_{21}, of our sample. Each torus consists of 10^4 consequents. In this dense coverage of the $\Delta x_0 = 0.4$ space away from the x_0 initial condition of the x1v1 p.o., we encountered only rotational tori nested around x1v1, until we reached V21. There, perturbing x_0 by $\Delta x_0 = 0.42$, the morphology of the torus changes. The V21 torus has a larger projection on the z-axis and does not follow anymore the pattern of the nested tori.

We repeat the same procedure at a larger energy, Ej=−4.39. This time the x initial condition of x1v1 is perturbed successively by $\Delta x = 0.1, 0.2, 0.3$ and 0.4. The result is given in Fig. 32, having a point of view $(\theta, \phi) = (27^o, 316^o)$. Four rotational tori surround the x1v1 p.o. and are indicated with arrows (U_1, U_2, U_3 and $U4$). Each torus consists of 10^4 consequents. The tori are distorted, with the last one having a morphology similar to V21 of the previous case.

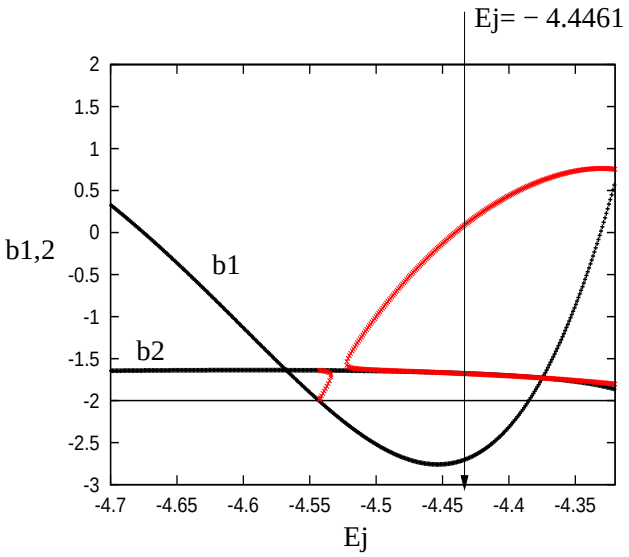

Fig. 33. Stability Diagram for $-4.7 < Ej < -4.3$, that shows the stability of the family x1 and its bifurcating family of p.o. x1v1.

6.2. *The small perturbation case* $q_a = 1.01, q_b = 1.0$

In order to study qualitative differences from the axisymmetric case when a small perturbation is introduced in the system, we increase the q_a parameter from $q_a = 1$ to $q_a = 1.01$. Fig. 33 gives for this system the evolution of the stability of the central family x1 and that of its bifurcations for $-4.7 <$ Ej < -4.3. We observe that x1 (b1, b2 indices with black lines) is initially stable and at Ej=−4.54 we have a transition from stability to simple instability. The family x1 becomes again stable at Ej=−4.386. At the transition from stability to simple instability x1v1 is bifurcated (red lines show its stability indices), as stable. At a larger energy (Ej=−4.525) we have a $S \to \Delta$ transition to complex instability of the family x1v1. In this case the stability indices become complex numbers and they do not appear

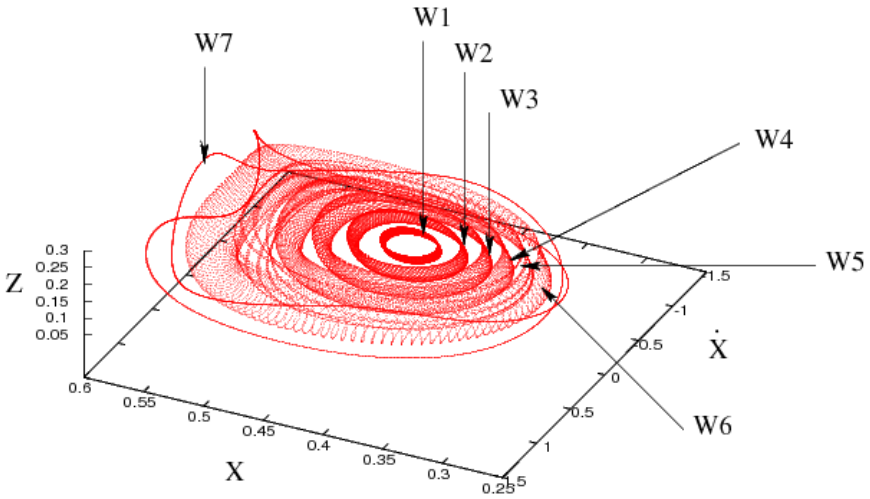

Fig. 34. The $(x, \dot{x}, z)$ 3D projection of the 4D surface of section for Ej=−4.4461 close to the stable p.o. x1v1. Our point of view is $(\theta, \phi) = (55^o, 194^o)$.

in the figure. There is a narrow complex unstable interval of x1v1 until Ej=−4.525, where x1v1 becomes again stable. In the present paper we study the phase space only in the neighborhood of stable p.o.

We choose a value of energy for which we have studied the orbital dynamics at the neighborhood of a stable x1v1 orbit at the axisymmetric case, Ej=−4.4461, and we perturb first he x_0 initial condition of x1v1 by $\Delta x = 0.02, 0.04 \ldots 0.14$ successively.

In Fig. 34 we observe seven tori at the $(x, \dot{x}, z)$ projection, which we name $W_1, W_2, \ldots W_7$, surrounding the fixed point of the x1v1 p.o. at this Ej. Each torus consists of 10^4 consequents. The morphology of W_1, W_2, W_3, W_4 and W_6 indicates that they are rotational while the morphology of W_5 and W_7 is typical for tube tori. The tubes of W_5 have many self-intersections. However, the gaps between them do not fill even if we consider 10^6 consequents. Thus, we conclude that W_5 is a tube torus. On the other hand, despite its wavy character, W_7 is a tube torus with only one self intersection in the 3D $(x, \dot{x}, z)$ projection. We note that tube tori appear in the 3D projections of the spaces of section as soon as a perturbation is introduced, even if it is a small one.

7. Summary and Conclusions

In this phenomenological paper we have studied in detail the structure of phase space in the neighborhood of stable periodic orbits in a 3D potential that represents a rotating, thick galactic disk. We have visualized the 4D spaces of section by means of the color and rotation method. This allowed us to clarify the properties of the invariant tori that we encounter in the vicinity of the stable p.o. We have also examined chaotic zones that we have found encaged between tori and the effect that these zones could have in the support of structures observed in thick galactic disks. Below we summarize our conclusions and compare our results with the results of previous studies.

(1) *On* the equatorial plane *(z=0)*, the dynamics of the system is determined by the presence of the central family x1. Even in the intervals that x1 is characterized as simple unstable *(U)*, we find in the $(x, \dot{x})$ surface of section invariant curves surrounding the periodic orbit.

(2) In general we find around stable periodic orbits invariant tori. In the *3D projections* we encounter the invariant tori that have been found in the papers by Froeschlé (1970, 1972), Martinet and Magnenat (1981), Contopoulos et al. (1982), Magnenat (1982), Patsis & Zachilas (1994) and Vrahatis et al. (1997), named by the latter authors "rotational tori". However, we have found as well the other kind of invariant tori, named by Vrahatis et al. (1997) "tube tori". The fact that this second kind of tori appear frequently in the vicinity of stable periodic orbits in totally different physical systems as are Hamiltonian systems of galactic type (this paper) and 4D symplectic maps associated with

the problem of beam stability in circular particle accelerators (Vrahatis et al. 1997), indicates that they represent a generic behavior in 3D orbits.

(3) The method of color and rotation was particularly enlightening in understanding the properties of the two kinds of tori.

- As regards the *rotational tori* in all cases we studied in our potential the continuation of color, that guarantees the smooth variation of the 4th coordinate, changes side along certain lines (Figs. 11, 12). This shows that *in the 3D projections* we have intersections in the rotational tori, which, in all cases we encountered in this study, appear four times on the tori.
- As regards the *tube tori*, their characteristic feature, the self-intersections of their tubes, was a projection effect in all cases, since at the intersections meet always different colors. We remark that we found always an odd number of self-intersections in the 3D projections of the tube tori. *In the 4D space* we did not find any self-intersections of the tube tori.

We found that the two kinds of tori cannot be distinguished neither from their rotation numbers, nor from the morphological features of the orbits in the configuration space.

(4) As we depart from the initial conditions of the stable p.o., the 3D projections of the tori appear distorted. Beyond a certain torus we found sticky chaotic orbits that for a long time remain on toroidal surfaces on which the consequents have a smooth color variation and finally diffuse in phase space, where we observe mixing of colors.

(5) We found chaotic orbits, which can be encaged by tori in the 4D space for times longer than a Hubble time, but not forever, since there are no topological barriers. We presented an example, where such orbits support a peanut morphology, similar but thicker than the morphology supported by the corresponding quasi-periodic orbits trapped around the stable x1v1.

(6) Tube-tori have been found only in the 3D projections of orbits in perturbed systems. In the axisymmetric case we encountered only rotational tori.

Acknowledgments We acknowledge many stimulating discussions and very useful comments from Prof. G. Contopoulos. We also acknowledge fruitful discussions with Prof. A. Pinotsis, Prof. M. Vrahatis and Dr. Ch. Skokos. This research has been partly supported by the Research Committee of the Academy of Athens under the project 200/739.

8. References

Abraham R. and Marsden J.E. [1978] *Foundations of Mechanics*, Benjamin-Cummings Publ. Co., Reading, Massachusetts.

Arnold V.I. and Givental A.B. [2000] "Symplectic Geometry" In: *Dynamical Systems IV*, ed by V.I. Arnold, S.P. Novikov, Springer-Verlag, New York Berlin Heidelberg, pp 1–138.

Arnold V.I. [1963] "Proof of a theorem of A.N. Kolmogorov on the invariance of quasi-periodic motions under small perturbations of the Hamiltonian" *Russ. Math. Surveys* **18**(5), 9-36.

Binney J. and Tremaine S. [2008] *Galactic Dynamics*, Princeton Univ. Press, Princeton.

Broucke R. [1969] "Periodic Orbits in the Elliptic Restricted Three-Body Problem" *NASA Tech. Rep.* 32-1360, 1-125.

Contopoulos G. [2002] *Order and Chaos in Dynamical Astronomy*, Springer-Verlag, New York Berlin Heidelberg.

Contopoulos G. and Papayannopoulos Th. [1980] "Orbits in weak and strong bars" *Astron. Astrophys.* **92**, 33-46.

Contopoulos G. and Barbanis B. [1985] "Resonant systems with three degrees of freedom" *Astron. Astrophys.* **153**, 44-54.

Contopoulos G. and Harsoula M. [2008] "Stickiness in Chaos" *Int. J. Bif. Chaos* **18**, 2929-2949.

Contopoulos G. and Patsis P.A. [2006] "Outer dynamics and escapes in barred galaxies" *Mon. Not. R. Astr. Soc.* **369**, 1039-1054.

Contopoulos G. and Magnenat P. [1985] "Simple three-dimensional periodic orbits in a galactic-type potential" *Celest. Mech.* **37**, 387-414.

Contopoulos G., Magnenat P. and Martinet L. [1982] "Invariant surfaces and orbital behavior in dynamical systems of 3 degrees of freedom II" *Physica D* **6**, 123-136.

Debattista V., Mayer L., Carollo C.M., Moore B., Wadsley J. and Quinn T. [2006] "The secular evolution of disk structural parameters", *Astrophys. J* **645**, 209-227.

Englmaier P. and Gerhard O.E. [1999] "Gas dynamics and large-scale morphology of the Milky Way galaxy" *Mon. Not. R. Astr. Soc.* **304**, 512-534.
Froeschlé C. [1970] "Numerical study of dynamical systems with three degrees of freedom" *Astron. Astrophys.* **4**, 115-128.
Froeschlé C. [1972] " Numerical study of a four-dimensional mapping" *Astron. Astrophys.* **16**, 172-189.
Hadjidemetriou J. [1975] "The stability of periodic orbits in the three-body problem" *Celest. Mech.* **12**, 255-276.
Kolmogorov A.N. [1954] "On the conservation of conditionally periodic motions under small perturbations of the Hamiltonian" *Dokl. Akad. Nauk USSR* **98**(4), 527-530.
Kuksin S. and Pöschel J. [1994] "On the Inclusion of Analytic Symplectic Maps in Analytic Hamiltonian Flows and its applications" In: *Seminars on Dynamical Systems*, ed by S. Kuksin, V. Lazutkin, J. Pöschel, Birkhäuser: Basel.
Magnenat P. [1982] "Numerical study of periodic orbit properties in a dynamical system with three degrees of freedom" *Celest. Mech.* **28**, 319-343.
Martinet L. and Magnenat P. [1981] " Invariant surfaces and orbital behavior in dynamical systems with 3 degrees of freedom." *Astron. Astrophys.* **96**, 68-77.
Lichtenberg A.J. and Lieberman M.A. [1992] *Regular and Chaotic Dynamics*, Springer-Verlag, Berlin Heidelberg New York.
Miyamoto M. and Nagai R. [1975] "Three-dimensional models for the distribution of mass in galaxies" *Publ. Astron. Soc. Japan* **27**, 533-543.
Moser J. [1962] "On invariant curves of an area preserving mappings of an annulus" *Nachr. Akad. Wiss. Gött, II Math.- Phys Kl.* 1-20.
Patsis P.A. and Grosbøl P. [1996] "Thick spirals: dynamics and orbital behavior" *Astron. Astrophys.* **315**, 371-383.
Patsis P.A. and Zachilas L. [1994] " Using Color and rotation for visualizing four-dimensional Poincaré cross-sections: with applications to the orbital behavior of a three-dimensional Hamiltonian system" *Int. J. Bif. Chaos* **4**, 1399-1424.
Patsis P.A., Skokos Ch. and Athanassoula E. [2002] "Orbital dynamics of three-dimensional bars-III. Boxy/peanut edge-on profiles" *Mon Not. R. Astr. Soc.* **337**, 578-596.
Pfenniger D. [1985a] " Numerical study of complex instability:I Mappings" *Astron. Astrophys* **150**, 97-111.
Pfenniger D. [1985b], "Numerical study of complex instability:II Barred galaxy bulges" *Astron. Astrophys.* **150**, 112-128.
Poincaré H. [1892] "Les Méthodes Nouvelles de la Mécanique Céleste" Gauthier Villars, Paris I (1892), II (1893), III (1899); Dover (1957).
Skokos Ch., Contopoulos G. and Polymilis C. [1997] "Structures in the phase space of a four dimensional symplectic map" *Celest. Mech. Dyn. Astron.* **65**, 223-251.
Skokos Ch., Contopoulos G. and Polymilis C. [1999] "Numerical study of the phase space of a four dimensional symplectic map" In *Hamiltonian Systems with three or more degrees of freedom*, ed. by Simó C., Plenum Press, p. 583-587.
Skokos Ch. [2010] "The Lyapunov characteristic exponents and their computation" *Lect. Notes Phys.* **790**, 63-135.
Skokos Ch. [2001] "On the stability of periodic orbits of high dimensional autonomous Hamiltonian systems" *Physica D* **159**, 155-179.
Skokos Ch., Patsis P.A. and Athanassoula E. [2002a] " Orbital dynamics of three-dimensional bars-I. The backbone of three-dimensional bars. A fiducial case" *Mon. Not. R. Astr. Soc.* **333**, 847-860.
Skokos Ch., Patsis P.A. and Athanassoula E. [2002b] "Orbital dynamics of three-dimensional bars-II. Investigation of the parameter space" *Mon. Not. R. Astr. Soc.* **333**, 861-870.
Vrahatis M.N., Bountis T.C. and Kollmann M. [1996] "Periodic orbits and invariant surfaces of 4D nonlinear mappings" *Int. J. Bif. Chaos* **6**, 1425-1437.
Vrahatis M.N., Isliker H. and Bountis T.C. [1997] "Structure and breakdown of invariant tori in a 4-D mapping model of accelerator dynamics" *Int. J. Bif. Chaos* **7**, 2707-2722.
Wiggins S. [2003] *Introduction to Applied Nonlinear Dynamical Systems and Chaos*, Springer-Verlag, Berlin Heidelberg New York.
Wolfram S. [1999] *The Mathematica book*, Wolfram media & Cambridge Univ. Press.